CEL in pancreatic disease: Do alcohol and smoking have an effect on the CEL-HYB1 protein?

Helene Nazmiye Pettersen

This thesis is submitted in partial fulfillment of the requirements for the degree of Master in Medical Biology.

Department of Biomedicine and Department of Clinical Medicine
University of Bergen,
Department of Medical Genetics
Haukeland University Hospital
June 2020

Table of Contents

Acknowledgments

First, I would like to extend my deepest gratitude toward my main-supervisor Dr. Karianne Fjeld. Your support, guidance and insightful comments throughout this year has been admirable and I truly appreciate being part of such an exciting project. You have pushed me to be independent and for that, I am very grateful.

Secondly, I would like to thank my co-supervisors Dr. Bente B. Johansson and Prof. Anders Molven. I would especially like to thank Bente for help in the lab, good discussion when it was needed and encouragement when experiments didn't work out. I especially like to thank Anders for all insightful remarks and comments during the writing process. Thank you, Anders, for sharing your knowledge with me.

I would also like to thank Anny Gravdal and Khadija El Jellas. Thank you Anny for always being helpful, giving me advice and for useful discussions about CEL. Thank you Khadija for all the help with immunohistochemistry; both helpful discussion, technical help and asking tough questions. I would also like to thank Solrun Steine for all help throughout this year.

I am very grateful towards all members of the Center for Diabetes Research for their kindness and for being welcoming towards me. I would also like to thank the Department of Medical Genetics and Molecular Medicine (MGM) and the Gade Laboratory for Pathology for laboratory space and for providing me with technical help.

I would like to thank my family for believing in me and supporting me. I would also like to thank my close friends for endless support. A special thanks to all my fellow master students for nice conversations and coffee breaks when it was needed.

Last, but certainly not least, I would like to thank Hans Marius Brandsdal Andersen. Your support and love throughout this year has been deeply appreciated.

Bergen, June 2020,

Helene Nazmiye Pettersen

Abbreviations

266-6 cells	Mouse pancreatic acinar tumor cells
AR42J cells	Rat pancreatic acinar tumor cells
BIP	Glucose-regulated protein 78 kDa
CEL/CEL	Carboxyl ester lipase gene/protein
CELP	Carboxyl ester lipase pseudogene
CSE	Cigarette smoke extract
dH_2O	Double deionized water
DMSO	Dimethyl sulfoxide
DNA	Deoxyribonucleic acid
E. coli	*Escherichia coli*
EDTA	Ethylenediaminetetraacetic acid
EtOH	Ethanol
ER	Endoplasmic reticulum
EV	Empty vector
GAPDH	Glyceraldehyde 3-phosphate dehydrogenase
GFP	Green fluorescent protein
HEK-293 cells	Human embryonic kidney cell line 293
HYB	Hybrid
kDa	Kilo Daltons
MODY	Maturity-onset diabetes of the young
NAHR	Non-allelic homologous recombination
o/n	overnight
T1D	Type 1 Diabetes
T2D	Type 2 Diabetes
TRUNC	Truncated artificial variant of *CEL* gene
UPR	Unfolded protein response
v/v	volume/volume
w/v	weight/volume
WT	wild type

Abstract

The digestive enzyme carboxyl ester lipase (CEL) is mainly expressed in the acinar cells of the exocrine pancreas. The protein contains a variable number of tandem repeats (VNTR) region, and the most common human form includes 16 VNTR repeats. We have previously identified disease-causing variants of CEL. One example is CEL-HYB1, which contains only 3 VNTR repeats and results in a truncated protein. Cellular studies of CEL-HYB1 have shown reduced secretion, intracellular accumulation and elevated ER stress compared to the normal CEL protein. Interestingly, *CEL-HYB1* is a genetic risk factor for chronic pancreatitis that act together with other risk factors to trigger disease development.

In this study, the main objective was to gain more insight into the disease mechanism of the CEL-HYB1 protein. More specifically, our aims were to study if environmental factors such as alcohol and cigarette smoking had any effect on the CEL-HYB1 protein by using both cellular and mouse models. Furthermore, we wanted to optimize a newly developed CEL-HYB1 specific antibody for immunostaining.

For most cellular studies on CEL, HEK-293 cells have been used, and with success. In this project, however, we wanted to use the mouse acinar cell line (266-6). But we found that both transfecting and detecting CEL protein expression in the 266-6 cells were challenging. Therefore, we optimized our research approach by transfecting the cells with V5-tagged CEL plasmids instead of untagged plasmids. By Western blotting we observed that CEL-HYB1 was less secreted compared to normal CEL, and also detected in the insoluble pellet fraction of transfected cells. By immunofluorescence, more intense intracellular signals were observed for CEL-HYB1 than for normal CEL. When the transfected 266-6 cells were treated with cigarette smoke extract (CSE) or ethanol (EtOH), there was a tendency of CEL-HYB1 increase in the pellet fraction when exposed to CSE. In contrast, we found no effect with EtOH.

In addition to cellular models, we used a humanized CEL-HYB1 *knock-in* mouse strain to do a pilot experiment by subjecting the animals to ethanol feeding. After 3 weeks of exposure, we observed no features of chronic pancreatitis when analyzing the mouse pancreas histology. Furthermore, we detected no signs of increased ER-stress when analyzing pancreatic lysates by Western blotting.

We tested the CEL-HYB antibody on cellular lysates from transfected 266-6 and HEK-293 cells, and from mice pancreases by Western blotting. In addition, mouse and human pancreatic

tissue was analyzed by immunohistochemistry. After optimization, the antibody worked for all experiments, except for analysis of the 266-6 cells by immunoblotting.

To summarize, we found reduced secretion and intracellular retention of CEL-HYB1 protein when expressed in 266-6 cells. This is similar to what has been reported in HEK-293 cells. We also observed CEL-HYB1 in the cell pellet fraction indicating CEL-HYB1 protein aggregation. When exposed to CSE, the level of CEL-HYB1 aggregation slightly increased. Finally, the CEL-HYB antibody was found to be specific for both Western blotting and immunohistochemistry and will serve as a useful tool for further CEL-HYB1 studies.

1. Introduction

1.1 The pancreas-anatomy and function

1.1.1The human pancreas

The human pancreas is a glandular organ located in the upper left part of the abdominal cavity, lying horizontally behind the stomach (Figure 1.1A). The gland has an elongated structure and can be divided into a head, body and tail region (Kumar et al., 2017). The pancreas can weigh 85-100 g (Caglar et al., 2014) and have a length of 15-20 cm in adults (Holck, 2019). It is the only organ in the body that contains an endocrine and an exocrine part. The endocrine pancreas consists of the islets of Langerhans, which produce hormones that are secreted into the bloodstream. The exocrine pancreas consists of acinar cells and the ductal system which produce, store and secrete digestive enzymes that are transported to the duodenum (Figure 1.1 B and C) (Kumar et al., 2017).

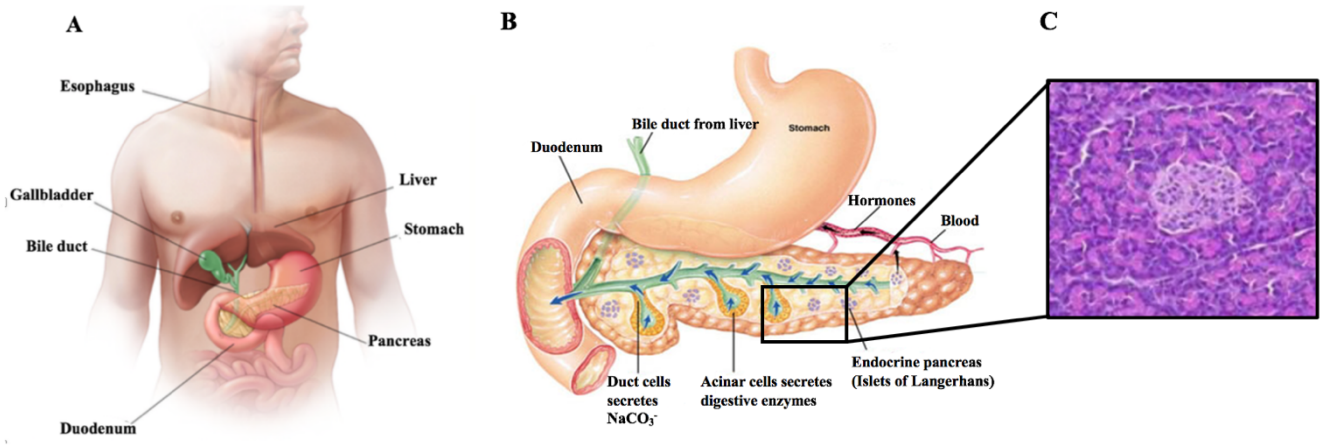

Figure 1.1 Anatomical overview, characteristics and histology of the pancreas. A) The human pancreas (yellow) is situated in the upper part of the abdominal cavity behind the stomach. Image from: https://www.mayoclinic.org/diseases-conditions/pancreatic-cancer/symptoms-causes/syc-20355421 **B)** The pancreas is divided into the endocrine and exocrine pancreas. The endocrine part consists of islets of Langerhans and secretes hormones while the exocrine part secretes digestive enzymes. Image from: https://socratic.org/questions/what-organ-functions-as-both-an-endocrine-and-exocrine-organ **C)** The image shows the histology of the pancreas where an islet of Langerhans (light pink) is surrounded by the acinar cells (dark pink/purple) of the exocrine pancreas.

1.1.2 The endocrine pancreas

The endocrine pancreas consists of groups of specialized cells arranged in clusters called islets of Langerhans (Kumar et al., 2017). The islets make up around 1-2 % of the total organ and are scattered within the exocrine tissue. The main function of the endocrine pancreas is to secrete hormones into the bloodstream (Roder et al., 2016). Each islet has a central core of beta cells (60 %) surrounded by alfa (30 %), delta, gamma and epsilon (together 10 %) cells (Figure 1.2) (Da Silva Xavier, 2018). The beta cells are responsible for the expression and secretion of the peptide hormone insulin while the alfa cells produce and release the peptide hormone glucagon. Both insulin and glucagon work to maintain a stable blood-glucose level. When the blood-glucose level rises, this will triggers the secretion of insulin to the bloodstream. The release of insulin stimulates an increased glucose uptake in muscle and other tissues and promotes the storage of glucose as glycogen in the liver. The result is a lowered blood-glucose level. Opposite, when the blood-glucose is low, glucagon is secreted. This results in the breakdown of glycogen into glucose to increase the concentration of blood-glucose (Lodish et al., 2016). The remaining cells of the islet of Langerhans, the delta, gamma and epsilon cells, produce the hormones somatostatin, pancreatic polypeptide and ghrelin, respectively (Da Silva Xavier, 2018).

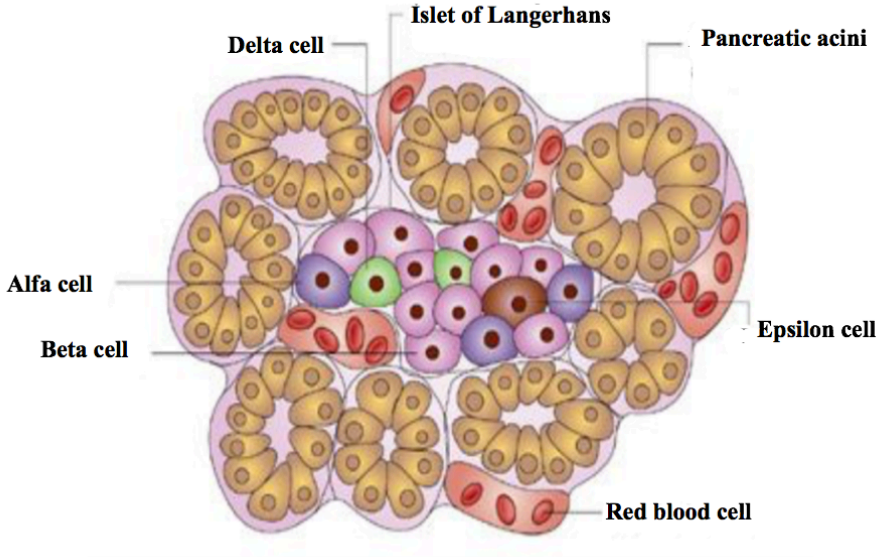

Figure 1.2 Schematic representation of the endocrine pancreas. Each islet of Langerhans is embedded within the exocrine tissue and consists of alfa, beta, gamma, delta and epsilon cells. The beta cells are the most abundant cell type and secrete and produce the hormone insulin, while the alfa cells secrete its antagonist glucagon. Figure adapted from: Bardeesy, N et al., 2002. *Nat Rev Cancer*

1.1.3 The exocrine pancreas

The exocrine part of the pancreas makes up around 95 % of the total organ and consists of acini and a ductal system (Das et al., 2014). Acini are clusters of acinar cells which are responsible for the production and secretion of digestive enzymes. The acinar cells produce digestive enzymes in an inactive form (zymogens) to prevent autodigestion and the enzymes are stored in zymogen granules before they are released (Figure 1.3). The digestive enzymes are classified based on their target substrates and include amylases, lipases, proteases and nucleases which break down carbohydrates, fats, proteins and nucleic acids, respectively. The enzymes are secreted from the acinar cells into ducts via interlobular ducts (Pandol., 2011). The ductal cells produce and secrete bicarbonate and water, which together with the digestive enzymes constitute the pancreatic juice. This juice is transported to the duodenum where it mixes with bile from the liver and chyme from the stomach (Lopez et al., 2019), having a key role in the digestion of food. Each day, the pancreas produces 2-3 liters of juice in an adult (Ishiguro et al., 2012). The exocrine cells in the pancreas has the highest level of protein synthesis in the adult body. Thus, the acinar cells have an extensive endoplasmic reticulum (ER) network (Logsdon et al., 2013).

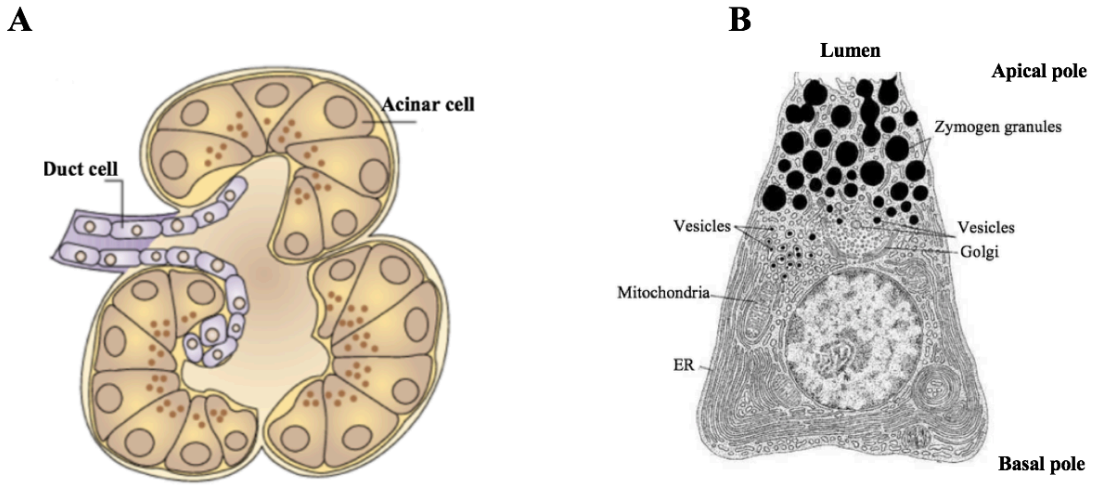

Figure 1.3 Schematic representation of the exocrine pancreas. A) An acinus is a cluster of acinar cells, which are in contact with the ductal system. The digestive enzymes are secreted into the lumen of the acinus and transported to the duodenum via the ducts. Figure adapted from: Bardeesy, N et al., 2002. *Nat Rev Cancer.* **B)** The acinar cells contain an extensive network of ER and mitochondria located at the basal pole. The digestive enzymes are stored in the zymogen granules located at the apical pole. Figure adapted from: www.zoology.ubc.ca//~berger/B200sample/unit_9_secretion/workshope9-htm

1.2. Diseases of the pancreas

The most common diseases of the pancreas are diabetes mellitus (commonly referred to as diabetes), neoplasms and inflammation (commonly referred to as pancreatitis).

1.2.1 Diabetes mellitus

Diabetes affects the endocrine part of the pancreas and is a group of metabolic diseases characterized by chronic hyperglycemia (Kumar et al., 2017). The disease is caused by defects in insulin secretion, insulin action or both. The majority of cases fall within two categories: type 1 diabetes (T1D) and type 2 diabetes (T2D) (American Diabetes Association, 2010). T1D makes up 5-10 % of all cases of diabetes and is an autoimmune disease resulting in beta-cell destruction and insufficient insulin production. Patients who suffer from T1D are often young when diagnosed (< 20 years) and they are dependent on insulin injections throughout life to control blood-glucose level (Kharroubi et al., 2015). Symptoms of T1D include increased thirst and appetite, fatigue and weight loss (Kahanovitz et al., 2017).

T2D is a multifactorial disease that accounts for about 90 % of all cases of diabetes cases. Both genetics and an unhealthy lifestyle are well-known risk factors and the disease is characterized by an onset between the ages of 30-40 years and a relative insulin deficiency (American Diabetes Association, 2010). Often, patients with T2D do not need insulin replacements to survive. A healthy diet and physical activity can be enough, especially at disease onset. Still, many T2D patients require medications to lower blood-glucose level (Marin-Peñalver et al., 2016). In addition to T1D and T2D, there are other forms of diabetes including gestational diabetes and monogenic diabetes. In gestational diabetes, hyperglycemia is detected during pregnancy whilst monogenic diabetes is caused by mutations in a single gene (American Diabetes Association, 2010).

Diabetes is the fifth leading cause of death worldwide and as of 2019, 422 million individuals worldwide suffers from this disease (World Health Organization., 2020). Within 2035, researchers believe this number will rise to almost 600 million (Forouhi et al., 2014).

1.2.2 Neoplasms of the pancreas

Neoplasms are divided into benign and malignant, where malignant neoplasm are collectively referred to as cancers. Neoplasms of the pancreas can originate from both the exocrine and the endocrine pancreas (Kumar et al., 2017). The most common type of pancreatic cancer is

pancreatic adenocarcinoma, which arise from the exocrine part and accounts for about 85 % of all cases (Hidalgo et al., 2015). Risk factors associated with pancreatic cancer are divided into two categories: modifiable and non-modifiable. The modifiable risk factors include smoking, alcohol, obesity and toxic substances. Smoking and alcohol are also risk factors for other pancreatic diseases including pancreatitis. Some of the non-modifiable risk factors are gender, age, ethnicity, diabetes, family history and certain gene variants (Rawla et al., 2019).

Worldwide, pancreatic cancer constitutes the seventh leading cause of cancer related deaths (Bray et al., 2018). In 2018, pancreatic cancer was the cause of more than 400,000 deaths worldwide accounting for 4.5 % of all cancer-related mortality. The prognosis for pancreatic cancer is poor as only 24 % of the patients survive one year after diagnosis (Rawla et al., 2019). Symptoms often include include jaundice, abdominal pain and weight loss (Kumar et al., 2017). Treatments for pancreatic cancer include surgical resection of the tumor, chemotherapy, radiation therapy and pain management (Vincent et al., 2011).

1.2.3 Pancreatitis

Pancreatitis is inflammation of the pancreas. The disease is usually divided into an acute and a chronic form (Kumar et al., 2017). The risk factors for acute pancreatitis include gallstones, alcohol, certain drugs, genetics and trauma, of which gallstones and alcohol abuse are the most common in adults (Forsmark et al., 2016). Acute pancreatitis is characterized by pancreatic swelling, fluid retention and pancreatic necrosis (Whitcomb, 2006). The pathogenesis of acute pancreatitis includes the autodigestion of the pancreas due to premature or inappropriately activation of digestive enzymes (Whitcomb, 2013).

Worldwide, the yearly incidence of acute pancreatitis is 34 per 100 000 in the general population (Petrov et al., 2019). An increase in acute pancreatitis incidences have been reported (Yadav et al., 2013). This may be due to more obesity as this condition can promote gallstone formation. The mortality of acute pancreatitis is about 2 % but this can increase to 30 % if patients are older and suffers from other diseases (Forsmark et al., 2016., Yadav et al., 2013). The symptoms of acute pancreatitis include abdominal pain, nausea and vomiting (Chatila et al., 2019). Patients with acute pancreatitis are given appropriate nutrition, pain management and intravenous hydration (Forsmark et al., 2016; Chatila et al., 2019). If a patient is suffering from several attacks from acute pancreatitis, this is called recurrent acute pancreatitis. Recurrent acute pancreatitis is again risk factor for developing chronic pancreatitis (Yadav et al., 2009) which will be described in detailed in the next section.

1.3 Chronic pancreatitis

Chronic pancreatitis is irreversible, long-standing inflammation of the pancreas that leads to permanent destruction of the pancreas parenchyma (Kleeff et al., 2017). The disorder is characterized by fibrosis, duct distortions, calcifications as well as pancreatic endocrine and exocrine dysfunction (Gardner et al., 2020). Symptoms of chronic pancreatitis are abdominal pain, weight loss, jaundice and maldigestion but the disease can also be clinically silent (Kumar et al., 2017). Patients who suffer from this disease also have an increased risk for the development of both diabetes and pancreatic cancer (Yadav et al., 2013). Treatment of chronic pancreatitis involves pain management, pancreatic enzyme replacements and proper diet. If the patient is smoking and/or suffering from alcohol abuse, cessation is necessary (Pham and Forsmark, 2018). However, currently, there is no cure for chronic pancreatitis (Kleeff et al., 2017).

The most common risk factors for chronic pancreatitis are recurrent attacks of acute pancreatitis, alcohol abuse, cigarette smoking and genetic predisposition (Kleeff et al., 2017). In western countries, alcohol abuse accounts for 40-70 % of all cases while cigarette smoking increases the risk for disease development in a dose-dependent manner (Lew et al., 2017). A study conducted by Yadav *et al*, found that five units of alcohol a day or more increased the disease risk (Yadav et al., 2009). In contrast, less than two drinks per day may have a protective effect against chronic pancreatitis as it has shown to inhibit a pro-inflammatory transcription factor (Lew et al., 2017).

Genetic risk factors for chronic pancreatitis include variants of the *PRSS1* (cationic trypsinogen), *CFTR* (cystic fibrosis transmembrane conductance regulator), *SPINK1* (serine protease), *CPA1* (carboxypeptidase A), *CTRC* (chymotrypsinogen C), and *CEL* (carboxyl ester lipase) genes (Mayerle et al., 2019). These risk factors can be further divided into various pathogenic pathways driving disease development and will be described in more detail in section 1.3.1. Among the genes listed above, three mutations in *PRSS1* are known to cause autosomal dominant hereditary pancreatitis (Saluja et al., 2019). The others are genetic risk variants that together with other risk factors (e.g. cigarette smoking or alcohol abuse) cause disease. Thus, most often, it is not a single factor but the combination of several risk factors that leads to chronic pancreatitis (Kleeff et al., 2017).

1.3.1 Disease mechanism of genetic risk in chronic pancreatitis

For more than a century, premature activation of pancreatic digestive enzymes was proposed to be the causative for pancreatitis (Saluja et al., 2019). In particular, inappropriate trypsin activity was the cornerstone for our understanding of pancreatitis as a disease characterized by autodigestion of the pancreatic tissue. Recently, new research has implemented new theories on the disease mechanism of chronic pancreatitis. These include risk factors that drive disease development through pathways alternative to uncontrolled digestive enzyme activation. Currently, three pathways are characterized namely the trypsin-dependent pathway, the misfolding-dependent pathway and the ductal pathway (Mayerle et al., 2019).

The trypsin-dependent pathway

This pathway involves pathogenic gene variants of *PRSS1*, *SPINK1* and *CTRC* that result in increased activation of trypsinogen, the precursor of trypsin, in the pancreas (Sahin-Toth, 2017, Hegyi and Sahin-Toth, 2017). *PRSS1* gene variants are often gain-of-function mutations that stimulate activation of trypsinogen either directly and indirectly (Hegyi and Sahin-Toth, 2017). Interestingly, three gene variants of *PRSS1* have shown to cause hereditary pancreatitis (Mayerle et al., 2019). Protective mechanisms that prevent trypsinogen activation include trypsin inhibition by SPINK1 and degradation of trypsinogen by CTRC. Consequently, loss-of function variants of both *SPINK1* and *CTRC* have shown to be associated with inappropriate trypsinogen activation and chronic pancreatitis development (Mayerle et al., 2019) .

The misfolding-dependent pathway

This pathway is related to gene variants that result in protein misfolding and endoplasmic reticulum (ER) stress (Mayerle et al., 2019). Elevated ER stress occurs when there is an imbalance between the folding of proteins and the functional demand that is placed on the ER. The stress may stem from alcohol, smoking, trauma or genetics, but either way it leads to an increase of BIP (GRP78) that binds to misfolded proteins within the ER lumen (Waldron et al., 2018). BIP sends downstream signal to three pathways: PERK (PKR like ER kinase), IRE1 (inositol-requiring protein-1) and ATF6 (activating transcription factor 6) which activate and promote the degradation of misfolded proteins, production of molecular chaperons and cell death (Cnop et al., 2017). These pathways all aid to restore homeostasis and are called the unfolded protein responses (UPR) (Alberts et al., 2015). Variants of *PRSS1, CPA1* and *CEL* have all been implicated in the misfolding-dependent pathway of chronic pancreatitis risk. In addition to increased ER-stress, expression of these genes leads to decreased protein secretion and intracellular protein retention in cellular systems (Mayerle et al., 2019).

The ductal pathway

The last pathway, namely the ductal pathway involves the *CFTR,* claudin 2 (*CLDN2*) and calcium-sensing receptor (*CASR)* gene variants. All these genes are expressed in pancreatic ductal cells (Mayerle et al., 2019). The C*FTR* gene encodes a chloride-bicarbonate channel and pathogenic variants in this gene disrupts the channel activity. The *CLDN2* encodes a tight junction protein in pancreatic ducts (Mayerle et al., 2019). Both, *CFTR* and *CLDN2* are important for secretion of chloride ions^{-} and bicarbonate. The *CASR* gene, encoding a receptor, responds to high levels of calcium in the pancreatic juice by increasing the secretion of ductal fluid (LaRusch and Whitcomb, 2011). Experimental evidence suggests that all three genes are important for proper secretion of the pancreatic juice. However, further studies are needed to fully understand their association with chronic pancreatitis (Derikx et al., 2015).

1.3.2 Model systems for studying chronic pancreatitis

Experimental research into chronic pancreatitis involves both cellular and animal models. The cellular models that are most commonly used are human embryonic kidney cells 293 (HEK-293) and rodent acinar cells (266-6: from mouse, AR42J: from rat). The HEK-293 cells have been a valuable tool since they are of human origin, easy to culture, maintain and transfect (Thomas et al., 2005). The downside of using HEK-293 is that they are not acinar cells. Furthermore, they are constitutively secretory cells and do not contain any zymogen granules or digestive enzymes. Therefore, the mouse tumor acinar (266-6) and the rat tumor acinar (AR42J) cell lines are in many respects more suitable model systems. These cell lines secrete digestive enzymes, can be transfected and provide a more suitable environment to study chronic pancreatitis However, as 266-6 and AR42J are cancer cell lines, they may exhibit different characteristics than normal acinar cells (Derikx et al., 2015)

Most of the animal models established to study chronic pancreatitis are rodents. The models of chronic pancreatitis can be divided into obstructive, environmental, chemical and genetic models (Lerch and Gorelick, 2013). Both partial, selective or complete pancreatic duct obstruction have been used to develop chronic pancreatitis in animals. The progression of disease is dependent on the species used and sometimes needs to be combined with stimulation of pancreatic secretion (Lerch and Gorelick, 2013). Chemical models for chronic pancreatitis involve the caerulein-induced method where rodents are injected with caerulein for several weeks (Lerch and Gorelick, 2013). Here, high frequency of caerulein injections causes pancreatic fibrosis (Aghdassi et al,. 2011). Intraperitoneal injections of ethanol to rodents can be used as an environmental model to study chronic pancreatitis. This method, however, does

not cause features characteristic of chronic pancreatitis alone, even with long-term administration. The administration of ethanol has to be combined with caerulein injections to cause pancreatic fibrosis (Lerch and Gorelick, 2013). This model has yet to be fully characterized but has proven to be an interesting in terms of understanding alcohol-induced effects on chronic pancreatitis.

Genetic models are important tools to study chronic pancreatitis (Lerch and Gorelick, 2013). Although some genetic manipulations can recapitulate the features shown in patients, the effects can be complex and vary greatly among species (Lerch and Gorelick, 2013). In a study by Geisz and Sahin-Toth, they analyzed *knock-in* mice with a variant of the cationic trypsinogen gene (Geisz and Sahin-Toth, 2018). They found many of the histological criteria for chronic pancreatitis in mouse including fibrosis, atrophy, metaplasia, dilated ducts and destruction of the acini. Eventually, they also observed destruction of the islets of Langerhans as shown in Figure 1.4 (Geisz and Sahin-Toth, 2018).

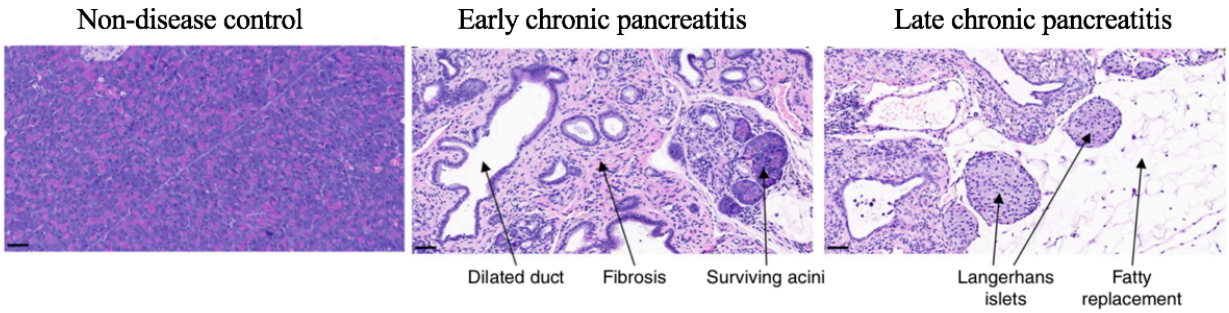

Figure 1.4 Histology of a genetic mouse model of chronic pancreatitis. In contrast to the control mouse (left), fibrosis, dilated ducts and fatty replacement was seen in both the early (middle) and late (right) stages of chronic pancreatitis. Figure adapted from: Geisz and Sahin-Toth, 2018. *Nat Communications.*

Another genetic model is the *CPA1 knock-in* mouse which develops chronic pancreatitis (Hegyi and Sahin-Toth., 2018). In a follow up study by Orekhova *et al,* they used *CPA1* homozygous mouse and exposed them to ethanol-feeding. Here, the *CPA1* mutant mice fed with ethanol showed an accelerated disease progression with a 2-fold higher histological score when comparing acinar cell loss (Orekhova et al., 2020).

1.4 Carboxyl ester lipase

Carboxyl ester lipase (CEL), a digestive enzyme also known as bile salt-stimulated lipase (BSSL) and bile salt-dependent lipase (BSDL) (Johansson et al., 2018), is mainly expressed in the acinar cells of the pancreas. CEL is one of three lipases secreted from this organ and it

makes up around 4 % of the total protein content of the pancreatic juice (Lombardo et al., 1978). The protein is synthesized and modified before stored in zymogen granules within the acinar cells. CEL is then secreted in an inactive form and transported to the duodenum (Whitcomb et al., 2007). Here, the enzyme is stimulated by bile salts and hydrolyses various substrates such as phospholipids, triacylglycerides, fat-soluble vitamins and cholesteryl esters (Lombardo and Guy, 1980). It has also been proposed that the CEL can degrade branched fatty acid esters of hydroxyl fatty acids, which are metabolites with anti-inflammatory and anti-diabetic effects (Kolar et al., 2016). In addition, CEL is expressed in lactating mammary glands and secreted with the mother's milk. Here, CEL has shown to be important for the digestion of fat in newborns (Blackberg et al., 1987, Lindquist and Hernell, 2010). CEL expression has also been detected at lower levels in macrophages (Kodvawala et al., 2005), eosinophils (Holtsberg et al., 1995) and endothelial cells (Li and Hui, 1998).

1.4.1 The human *CEL* gene

The human *CEL* gene is about 10 kb in size and located on the long arm of chromosome 9q34.13. The gene consists of 11 exons (Figure 1.5) where the last exon contains a variable number of tandem repeat (VNTR) region (Taylor et al., 1991, Lidberg et al., 1992). The repeats are nearly identical 33 bp segments that encode 11 amino acids each. The most common number of VNTR repeats is 16, although it ranges between 3 to 23 repeats (Torsvik et al., 2010, Fjeld et al., 2016).

Situated 11 kb downstream of the *CEL* gene is the *CEL* pseudogene (*CELP*) (Lidberg et al., 1992). Compared to *CEL*, the *CELP* gene is missing exon 2-7 of *CEL* and contains a stop codon in exon 8 (Figure 1.5). Otherwise, the two genes share 97 % sequence similarities. The *CELP* gene is probably not transcribed into a protein due to the premature stop codon in exon 7.

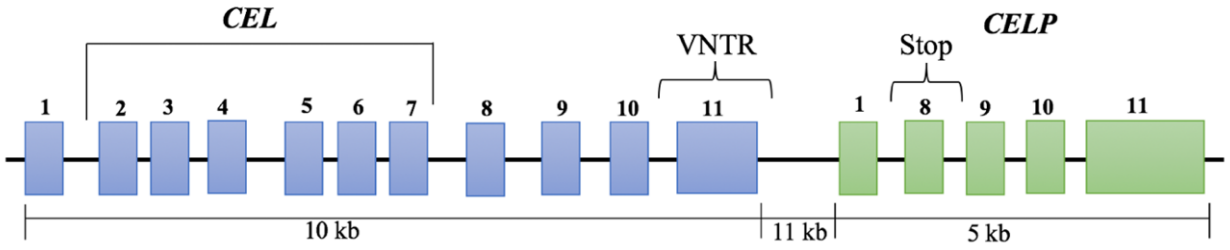

Figure 1.5 The gene structure of *CEL* and its neighboring pseudogene *CELP*. The *CEL* gene (blue) is about 10 kb in size and is situated next to its pseudogene *CELP* (green). The genes are located on chromosome 9. Exons 2-7 are only present in the *CEL* gene as indicated in the figure. VNTR; variable number of tandem repeat region. Drawn after: Fjeld et al., 2015. *Nat Genet*

1.4.2 The CEL protein and secretion

The CEL protein has two structural domains; an N-terminal globular domain that contains the catalytic site, bile salt binding sites and a signaling peptide, and a C-terminal region with the VNTR domain (Figure 1.6) (Reue et al., 1991, Terzyan et al., 2000, Holmes and Cox, 2011). The bile salt binding sites are located within the globular domain of the protein as is the catalytic triad of Ser194-His435-Asp320 (Holmes and Cox, 2011). The VNTR region contains enrichments of the amino acids proline (P), glutamate (E), serine (S) and threonine (T) (Figure 1.6). This is known as a PEST sequence and is found to play a key role in protein degradation as it is observed in many short-lived proteins (Rogers et al., 1986).

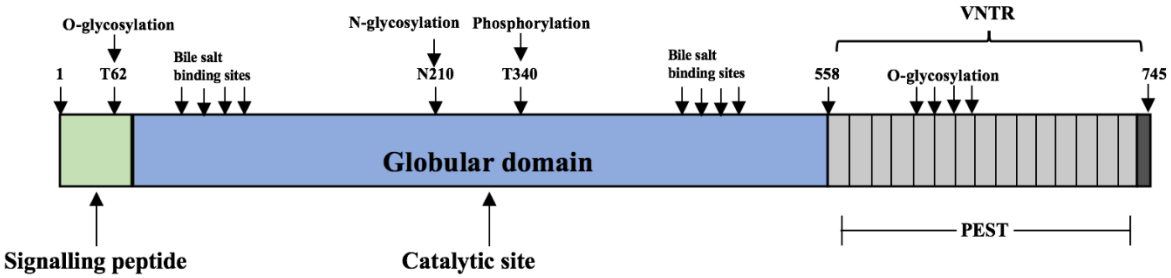

Figure 1.6 The protein structure of CEL. The protein comprises two structural domains: the N-terminal globular domain containing both the signaling peptide (green) and the catalytic domain (blue), and the C-terminal VNTR region (grey). The figure also shows binding sites for bile salts, O-glycosylation, N-glycosylation, phosphorylation, and the PEST sequence. Drawn after: Johansson et al., 2018. *Pancreatology*

CEL is found to be a conserved protein that is a member of the α/β hydrolase family (More et al., 2011). Around 11 β-sheets makes up the core, which is surrounded by 15 α-helices (De Jaco et al., 2016). The CEL protein has a predicted molecular weight of 79 kDa and contains the distinctive C-terminal tail sequence KEAQMPAVIRF (Johansson et al., 2018).

In the acinar cells, CEL follows the classical pathway of secretory proteins (Lombardo, 2001). The N-terminal hydrophobic signaling peptide of CEL directs the protein from the nucleus to the ER. Here, CEL is N-glycosylated at asparagine position 210, N210 (Figure. 1.6) (Aboukali et al., 1993). The protein is then relocated to the Golgi in association with a protein complex that contains the molecular chaperone GRP94 (glucose regulated protein, 94 kDa) (Bruneau et al., 1995). In the Golgi apparatus the protein is heavily O-glycosylated at both serine and threonine residues within the PEST sequence (Bruneau et al., 1997) (Figure. 1.6). The O-glycosylation of CEL is important for the protein's integrity as proteins lacking O-glycosylation are less secreted and more prone for degradation (Bruneau et al., 1997). As PEST sequences are observed in many short-lived proteins, there is a possibility that O-glycosylation is most likely masking the PEST sequences in CEL to prevent degradation (Rogers et al., 1986, Loomes et al., 1999).

Once phosphorylated on threonine residue 340, CEL is released from the Golgi and stored as an inactive enzyme in the zymogen granules (Pasqualini et al., 2000). Upon stimulation, CEL is excreted from the luminal face of the acinar cells and transported to the duodenum.

1.5 Pathogenic variants of CEL

1.5.1 CEL-MODY

CEL-MODY (MODY8) is an autosomal dominant inherited disease. In addition to diabetes, the patients are clinically characterized by a slowly progressing pancreatic exocrine dysfunction that includes both lipomatosis and the development of pancreatic cysts (Johansson et al., 2018).

CEL-MODY is caused by single-base deletions in the first or fourth repeat within the *CEL*-VNTR region. The mutations lead to a frameshift and a premature stop codon in VNTR repeat 11 and 13, respectively (Ræder et al., 2006). The variants were identified in two independent families from Norway. However, CEL-MODY is a very rare disease. In addition to the Norwegian pedigrees, only two other families have been discovered: one from Sweden and one from the Czech Republic (unpublished).

Compared to the CEL-WT protein with a theoretical size of 79 kDa, the CEL-MODY proteins have a truncated C-terminal and a predicted size of about 73 kDa. Cellular studies from our research group indicate that CEL-MODY variants cause a protein-misfolding disease as this variant has a tendency to form aggregates both inside and outside the cell (Johansson et al., 2011, Torsvik et al., 2014, Gravdal et al, unpublished). In addition, the CEL-MODY protein is less secreted and induces ER-stress when expressed in both HEK-293 and rat AR42J acinar cells (Xiao et al., 2016, Gravdal et al,unpublished). Recent studies have also shown that once secreted, the CEL-MODY protein can be taken up by neighboring cells and induce cell death (Torsvik et al., 2014, Dalva et al., 2020).

1.5.2 CEL-HYB

In 2015, our research group reported *CEL-HYB* as a novel genetic risk factor for chronic pancreatitis (Fjeld et al., 2015). In this study, cohorts of idiopathic chronic pancreatitis from both France and Germany were analyzed and CEL-HYB was overrepresented by five-fold in cases compared to healthy controls. The *CEL-HYB* allele was also found to be enriched in patients with alcohol-induced chronic pancreatitis (Fjeld et al., 2015).

CEL-HYB is a deletion hybrid variant that has most likely originated from a process called non-allelic homologous recombination (NAHR) between the *CEL* gene and the *CEL* pseudogene (*CELP*) (Fjeld et al., 2015). NAHR is a mechanism in which the cells aim to repair broken chromosomes resulting in gross genome rearrangements (Parks et al., 2015). NAHR usually happens between two genes that share a high sequence similarity, which is the case for *CEL* and *CELP* that share about 97 % sequence similarity in the common sequences. In addition to the deletion hybrid allele (*CEL-HYB*), the process has led to the formation of a reciprocal duplication allele (*CEL-DUP*) as illustrates in Figure 1.7 (Fjeld et al., 2015).

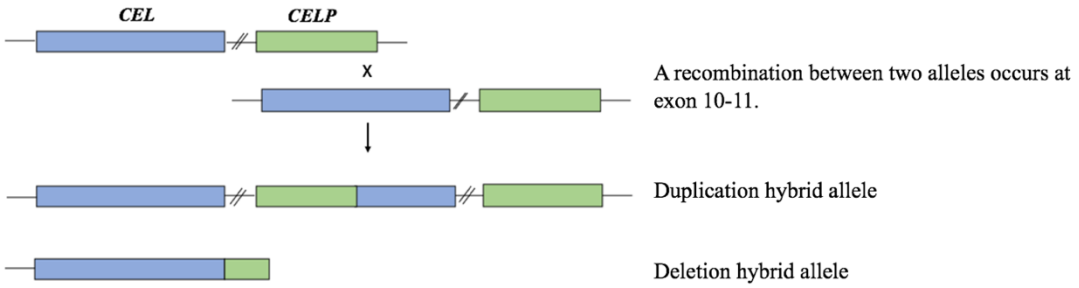

Figure 1.7. Proposed mechanism of how the *CEL-HYB1* gene originated through non-allelic homologous recombination. The X symbolizes the crossover event in the exon 10–exon 11 regions of *CEL* and *CELP*. The resulting alleles are the duplication hybrid allele (*CEL-DUP*) and the deletion hybrid allele (*CEL-HYB*). Drawn after: Fjeld et al., 2015. *Nat Genet.*

The *CEL-HYB* gene encodes a chimeric protein where the globular domain is identical to the CEL-WT protein while the C-terminal VNTR region with only three repeats originates from *CELP* (Fjeld et al., 2015). When expressed in HEK-293 cells the CEL-HYB protein showed impaired secretion, induced autophagy and intracellular accumulation compared to CEL-WT (Fjeld et al., 2015). CEL-HYB was also found to have a 40 % reduced enzyme activity level compared to CEL-WT (Fjeld et al., 2015). Furthermore, in an unpublished study by our group, CEL-HYB showed induced ER-stress when expressed in HEK-293 cells (Tjora et al., unpublished). Based on these recent findings, we can now conclude that *CEL-HYB* belongs to the misfolding-dependent pathway of genetic risk in chronic pancreatitis (Tjora et al., unpublished).

In contrast to the European cohorts, the *CEL-HYB* allele was not found to be associated with chronic pancreatitis in three independent cohorts from Japan, India and China, respectively (Zou et al., 2016). Actually, they found no *CEL-HYB* positive samples, but discovered an alternative *CEL-HYB* allele which they designated *CEL-HYB2* (to distinguish it from the first identified *CEL-HYB* allele, which was renamed *CEL-HYB1*). The *CEL-HYB2* allele was detected in all three Asian populations but exhibited no association with chronic pancreatitis. Compared to *CEL-HYB1*, *CEL-HYB2* has a premature stop codon located in exon 10 that most likely results in nonsense-mediated mRNA decay (Nickless et al., 2017). Consequently, the expression and secretion of the CEL-HYB2 protein is predicted to be reduced as illustrated in Figure 1.8 (Zou et al., 2016, Molven et al., 2016).

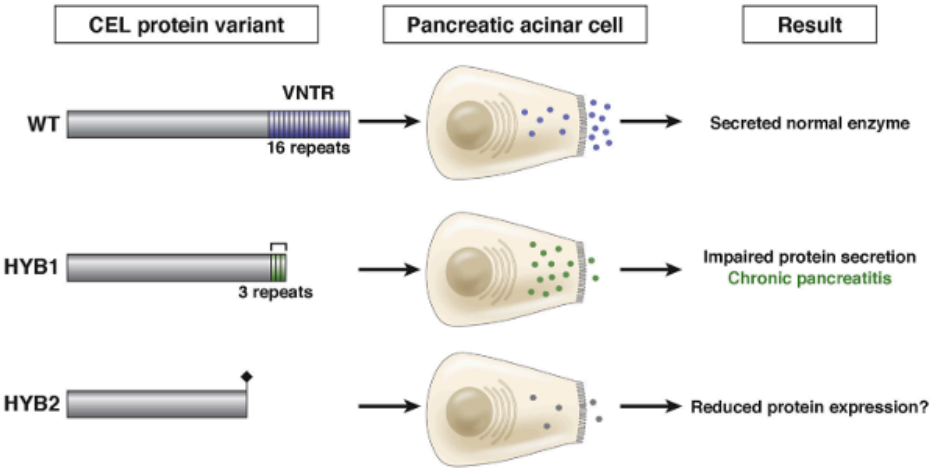

Figure 1.8. C-terminal and cellular characteristics of CEL-HYB1 and CEL-HYB2 compared to CEL-WT. The most common CEL-WT protein usually consists of 16 repeats in the VNTR region. The CEL-HYB1 variant contains only 3 VNTR repeats that originates from the *CEL* pseudogene. CEL-HYB1 is not secreted efficiently and leads to an increased risk for chronic pancreatitis. The CEL-HYB2 variant has a premature stop-codon before the VNTR region. This results in nonsense-mediated mRNA decay and probably a reduced protein expression. The CEL-HYB2 variant is not associated with chronic pancreatitis. Figure is adapted from: Molven et al., 2016. *Gastroenterology.*

Based on the results from the Asian populations, Zou *et al* suggested that the *CEL-HYB1* allele is an ethnic-specific risk factor for chronic pancreatitis (Zou et al., 2016). To follow up on that, a recent study analyzed the *CEL-HYB1* allele in a cohort consisting of pediatric chronic pancreatitis patients from Poland. Here, the frequency of *CEL-HYB1* was found to be twice as high in cases compared with the control group although the difference did not reach statistical significance (Oracz et al., 2019).

Compared to CEL-MODY, which results in a dominantly inherited, high-penetrant disease, *CEL-HYB1* is "only" a risk factor for chronic pancreatitis. Thus, in *CEL-HYB1* positive families the allele follows an autosomal dominant inheritance pattern with incomplete penetrance (Fjeld et al., 2015, Oracz et al., 2019). Furthermore, a relatively large number of healthy individuals are *CEL-HYB1* positive. In the European populations studied so far, between 0.3 - 2.5% of the general population is estimated to carry the risk allele without being sick (Fjeld et al., 2015, (Dalva et al., 2016, Oracz et al., 2019). This indicates that it is not *CEL-HYB* alone that causes disease – it is *CEL-HYB1* in combination with other chronic pancreatitis risk factors that triggers disease.

2. Aims

The overall aim of this study was to gain more insight into the disease mechanism of the CEL-HYB1 protein.

The specific aims were:

1. To investigate the effect of cigarette smoking extract and alcohol on CEL-HYB1-transfected mouse acinar cells

2. To examine the effect of ethanol-feeding on a humanized CEL-HYB1 *knock-in* mouse strain.

3. To test the specificity of a newly developed CEL-HYB antibody by using cell lysates, and mouse and human tissue samples

3. Materials

Table 3.1 Plasmids

Plasmid*	Encoding	Description
pcDNA 3.1-CEL-WT/V5-His	CEL-WT	Plasmid expressing the CEL wild type (WT) protein containing 16 VNTR repeats (Johansson et al., 2011)
pcDNA 3.1-CEL-HYB1/V5-His	CEL-HYB1	Plasmid expressing the CEL-HYB1 protein (Fjeld et al., 2015)
pcDNA 3.1CEL-TRUNC/V5-His B	CEL-TRUNC	Plasmid expressing CEL-TRUNC, an artificial CEL protein lacking the VNTR domain (Johansson et al., 2011)
pcDNA 3.1.CEL-HYB1^{N}/V5-His	CEL-HYB1^{N}	Plasmid expressing CEL-HYB1 where an N-glycosylation site has been mutated in the C-terminal of the protein. New name: CEL-HYB1^{N} (unpublished)
pcDNA 3.1/V5-His	EV	Empty vector

*All plasmids are based on the mammalian expression vector pcDNA3.1/V5-His B from Invitrogen

Table 3.2 DNA methods

Product	Catalog number	Supplier
Ampicillin	A9518-5G	Sigma Aldrich
*Bam*HI restriction enzyme	R0136S	New England BioLabs
CutSmart Buffer	B7204S	New England BioLabs
OneShot TOP10 Chemically Competent *E.coli* cells	C4040-03	Invitrogen
Ethidium bromide	E1510-10ml	Sigma Aldrich
Gel Loading Dye, Blue (6X)	B7021S	New England BioLabs
imMedia Amp Agar	45-0034	Invitrogen
Lysogeny broth (LB) medium	SLBQ7430V	Sigma Aldrich
NuSieve 3-1 Agarose	7894	Lonza
QIAfilterPlasmid Midi Kit (100)	12245	Qiagen
TE buffer (pH 8.0)	AM9849	Invitrogen

Table 3.3 Cell lines

Cell line	Description	Catalog number	Supplier
266-6	Mouse pancreatic acinar tumor cell	CRL-2151	ATCC
HEK-293	Human embryonic kidney cells 293	632180	CloneTech Laboratories

Table 3.4 Cell culturing

Product	Catalog number	Supplier
Antibiotic Antimycotic	15240062	Thermo Fischer Scientific
Dimethyl sulfoxide (DMSO)	D8418-250ml	Sigma-Aldrich
Dexamethasone	D4902-25MG	Sigma-Aldrich
Dulbeccos Modified Eagles medium	41966-029-500ml	Gbco by Life Technologies
Dulbeccos Phosphate Buffered Saline	RNBH2629	Sigma Aldrich
Fetal Bovine Serum (FBS)	F7524-500ml	Sigma Aldrich
0.05 % Trypsin EDTA (1x)	253000-054 -50ml	Gibco by Life Technologies

Table 3.5 Transient transfection and treatment of cells

Product	Catalog number	Supplier
Amaxa SF Cell line 4D Nucleofector X Kit L	V4XC-2024	Lonza
Cigarette smoke extract (CSE)	-	Murty Pharmaceuticals
Lipofectamine 2000 Reagent	11668019	Invitrogen
Nunclon Delta Surface 6 well plates	140675	Thermo Scientific
Opti-MEM Reduced Serum Medium	31985062	Thermo Fisher Scientific
RPMI 1640 Medium	11875093-500ml	Thermo Fisher Scientific

Table 3.6 Cell lysis, SDS-PAGE and Western blotting

Product	Catalog number	Supplier
Amersham Hybond 0.45 µm PVDF membrane	10600029	GE Healthcare Life Science
Blocking grade blocker nonfat-dry milk	170-6404	BioRad
Blotto, nonfat-dry milk	sc-2324	Santa Cruz Biotechnology Inc
Magic Mark XP Western Protein Standard	LC6502	Invitrogen
Methanol	67-56-1	Merck Millipore
NuPAGE LDS sample buffer (4x)	NP0007	Thermo Fisher Scientific
NuPAGE MOPS SDS running buffer (20x)	NP0001-01	Thermo Fisher Scientific
NuPAGE Novex 4-12 % Bis-Tris protein gels (1 mm, 10 wells)	NP0321BOX	Thermo Fisher Scientific
NuPAGE Novex 10% Bis-Tris protein gels (1 mm, 10 wells)	NP0301BOX	Thermo Fisher Scientific
NuPage Transfer Buffer (20X)	NP0006-1	Thermo Fisher Scientific
NuPAGE Sample reducing agent (10x)	NP0009	Thermo Fisher Scientific
Phosphate buffer saline (PBS) tablets	18912-014	Gibco
Pierce BCA protein assay kit	23225	Thermo Scientific
Pierce ECL Plus Western Blotting Substrate	32132	Thermo Scientific
Precision Plus Protein dual color standard	161-0374	Biorad
Restore Western blot stripping buffer	21059	Thermo Scientific
β-mecaptoethanol	60-24-2	Sigma Aldrich
RIPA lysis buffer (10x)	20-188	Merck Millipore

Table 3.7 Immunofluorescence

Product	Catalog number	Supplier
ProLong Gold Antifade Mountant with DAPI	P36935	Molecular Probes
Normal goat serum	1000C	Invitrogen
Nunclon Delta Surface 12 well plates	150628	Thermo Scientific
Paraformaldehyde (PFA)	818715	Merck Millipore
Poly-L-Lysine	RNBD9368-10ml	Gibco by Life Technologies
Duran group microscope slides	23 550 13	Duran Group

Table 3.8 Immunohistochemistry

Product	Catalog number	Supplier
DAKO pen	S2002	Agilent DAKO
Envision Flex Hematoxylin	K8008	Agilent DAKO
Normal goat serum (10 %)	50197Z	Thermo Fisher Scientific
Pertex Mounting Media	00811-EX	Histolab
Liquid DAB+ Substrate Chromogen System	K3468	Agilent DAKO
Target Retrieval Solution, pH 9.0, 10x	S2367	DAKO
Target Retrieval Solution, Citrate pH 6.0 10x	S2031	DAKO

Table 3.9 Primary antibodies

Antibody	Catalog number	Supplier	Method
Anti-CEL (rabbit polyclonal)	Gift (Xiao et al., 2016)	Prof. Mark E. Lowe, Washington University School of Medicine, St. Louis, USA	Western Blot
Anti-CEL (rabbit polyclonal)	SAB2103782	Sigma-Aldrich	Western Blot
Anti-CEL (rabbit polyclonal)	HPA052701	Sigma-Aldrich	Immunohistochemistry
Anti-BIP (rabbit polyclonal)	Ab21685	Abcam	Western Blot
Anti-GAPDH (goat polyclonal)	Sc-47724	Santa Cruz Biotechnology Inc	Western Blot
Anti-V5 (mouse monoclonal)	46-0705	Invitrogen	Western Blot and Immunofluorescence
Anti-CEL-HYB (rabbit polyclonal)	Designed by the Bergen group	Davids Biotechlogie	Western Blot and Immunohistochemistry
Anti-Actin (mouse monoclonal)	A5441	Sigma Aldrich	Western blot

Table 3.10 Secondary antibodies

Antibody	Catalog number	Supplier	Method
Goat anti-Rabbit IgG HRP	65-6120	Thermo Fisher	Western Blot
Donkey anti-Mouse IgG HRP	Sc-2306	Santa Cruz Biotechnology Inc	Western Blot
Mouse anti-Goat IgG HRP	Sc-2354	Santa Cruz Biotechnology Inc	Western Blot
Donkey anti-Goat IgG HRP	Sc-2020	Santa Cruz Biotechnology Inc	Western Blot
F(ab´)2-Goat anti Mouse IgG (H+L) Cross-Adsorbed Secondary Antibody, Alexa Fluor 488	A-11017	Thermo Fischer Scientific	Immunofluorescence
MACH3 Rabbit HRP-conjugated Polymer	RH531H	Biocare Medical	Immunohistochemistry
MACH3 Rabbit Probe	RP531H	Biocare Medical	Immunohistochemistry

Table 3.11 Buffers and solutions

Buffer	Method	Composition
TBE buffer (pH 8.3)	Gel electrophoresis	Tris-borate (45 mM) and EDTA (1 mM)
NuPAGE MOPS SDS running buffer (1x)	SDS-PAGE	For 1 L: 50 ml NuPAGE ® MOPS 20x in 950 ml dH_20.
NuPAGE Transfer Buffer (1x)	Western Blot	For 1L: 50ml NuPAGE ® Transfer buffer (20x) in 850 ml dH_2O and 100 ml methanol.
5 % milk in PBS-T (0.05 %)	Western blot	2.5 g blocking grade blocker nonfat-dry milk in 50 ml PBS-T (0.05 %).
PBS-T (0.05 %)	Western blot	For 1 L: 2 tablets of PBS dissolved in 1L dH_2O with 0.05% Tween ® 20.
RIPA lysis buffer	Cell lysis (cells)	10x RIPA lysis buffer (0.5 M Tris-HCl, 1.5 M NaCL, 2.5 % deoxycholic acid, 10 % NP-40, 10 mM EDTA, pH 7.4) + 1 tablet

		Complete™ Mini EDTA-free protease inhibitors cocktail tablet
RIPA lysis buffer	Cell lysis (tissue)	1x RIPA lysis buffer (25 mM Tris, 150 mM NaCl, 1 % Triton X-100, 1 % sodium deoxycholate, 1 % SDS, pH 7.6) + 1 tablet Complete Mini EDTA-free protease inhibitors cocktail tablet
Blocking buffer	Immunofluorescence	5 % normal goat serum in washing buffer
Washing buffer	Immunofluorescence	For 1 L: 2 tablets of PBS in 1 L dH_2O.
Permeabilization buffer	Immunofluorescence	15 µl Triton X-100 and 15 µl Tween 20 dissolved in 14.7 ml PBS.
Fixative	Immunofluorescence	6 % paraformaldehyde in 3 ml 1x Phosphate buffered saline
Citrate-EDTA buffer (10 mM citric acid, 2 mM EDTA and 0.05 % Tween)	Immunohistochemistry	For 1 L: 1.92 g citric acid and 0.74 g EDTA in 1000 ml dH_20. pH adjusted to 6.2 and addition of 0.5 ml Tween
Sodium citrate buffer (10 mM sodium citrate and 0.05 % Tween)	Immunohistochemistry	For 1 L: 2.94 g tri-sodium citrate added to 1000 ml dH_20. pH adjusted to 6 and addition of 0.5 ml Tween.
Glycine buffer (0.05 mM glycine)	Immunohistochemistry	For 1 L: 3.75 g glycine to 1000 ml dH_20 (pH 3.5). Mix 200 ml glycine buffer with 5.7 ml 1M HCl.
High salt antibody diluent	Immunohistochemistry	0.05 M Tris, 0.15 M NaCl, 1 % BSA, 0.015 M Na-azide and 0.05 % Tween. Adjust pH to 7.4
Low salt antibody diluent	Immunohistochemistry	0.05 M Tris, 0.075 M NaCl, 1 % BSA, 0.015 M Na-azide and 0.05 % Tween. Adjust pH to 7.4
Endogen peroxidase blocking solution	Immunohistochemistry	3 % (v/v) H_2O_2 in dH_2O

3.1 Animals

Our research group has recently developed a humanized *knock-in* CEL-HYB1 mouse strain. The transgenic strain was made on the C57BL/6J background by GenoWay, Lyon, France, by using the Cre/LoxP system.

A schematic representation of how the CEL-HYB1 strain was generated is shown in Figure 3.1. Only heterozygous CEL-HYB1 mice were used in this project. C57BL/6J (0/0) was used as

controls. Heterozygous CEL-HYB1 mice (0/ki) harbor the three VNTR repeats from the human *CEL-HYB* allele on one *Cel* allele and a normal mouse *Cel* gene on the other.

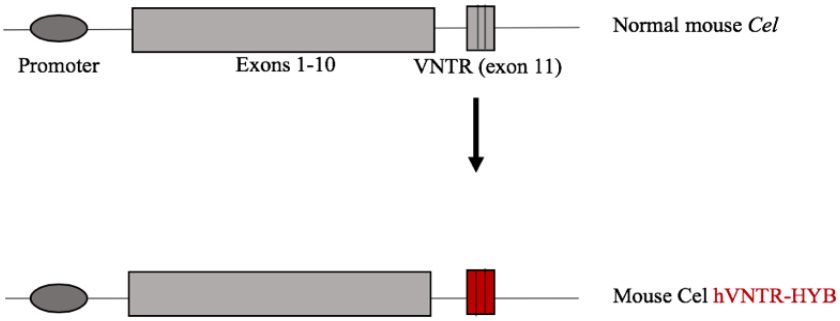

Figure 3.1 Schematic representation of how the CEL-HYB1 mouse strain was generated. The mouse *Cel* VNTR was replaced by the human VNTR of *CEL-HYB1* **(**Fjeld et al., 2015**).**

Table 3.12 Mice work

Product	Catalog number	Supplier
Trident RIPA lysis buffer	GTX400005 100 ml	GenTex
Rodent Liquid Diet Lieber-DeCarli 82 Shake and Pour Control Diet	F1259SP	Bio-Serv
Rodent Liquid Diet Lieber-DeCarli 82 Shake and Pour Ethanol Diet	F1258SP	Bio-Serv
Liquid Diet Feeding Tubes	#9019	Bio-Serv

Table 3.13 Technical equipment

Product	Supplier
NanoDrop ND-1000	Thermo Scientific
Sceptre 2.0 handheld automated cell counter	Millipore
Countess II Automated Cell counter	Thermo Fisher Scientific
Leica Confocal SP8	Leica Microsystems
Leica DM200 LED	Leica Microsystems
ChemiDoc MP Imaging System	BioRad
Gen 5 2.06 software	Biotek
Eppendorf centrifuge 5417C	A/B Phil
Heraeus multifuge 3S-R	Thermo Electron corporation
Heraeus Fresco 21 Microcentrifuge	Thermo Fisher Scientific
Heraeus Megafuge 1.0	Thermo Fisher Scientific
4D-Nucleofector System	Lonza
Virsonic 300 UltrasonicCell Disrupter, 1/8” micro probe tip, 400W	Virtis

Table 3.14 Analytical software

Product	Supplier
LASV4.8	Leica Microsystems
FIJI software	ImageJ
LAS X software	Leica Microsystems
Image Lab 6.0.1 Software	BioRad

4. Methods

4.1 Plasmid preparation

4.1.1 Transformation of OneShot TOP10 Chemically Competent *E.Coli* cells

Transformation was conducted by a rapid chemical procedure as described by the manufacturer (Invitrogen). In brief, pcDNA3.1 plasmids encoding different CEL-variants (Table 3.1) were transformed into OneShot TOP10 Chemically Competent *E. coli* cells. One µl of plasmid (500-1000 ng) was added to 25 µl of *E. coli* cells. The cells were spread onto pre-warmed (37 °C) agar plates containing the selection marker ampicillin (100 µg/ml) and incubated overnight (o/n) at 37 °C.

4.1.2 Bacterial glycerol stocks and plasmid purification

For each transformation, a single bacteria colony was picked and inoculated into a 25 ml culture of lysogenic broth (LB) medium containing ampicillin (100 µg/ml). The culture was incubated o/n at 37 °C with shaking at 250 rpm. A bacterial glycerol stock was made for each plasmid by diluting 500 µl of the bacteria culture with 500 µl of 50 % glycerol. The stocks were stored at -80 °C. For plasmid preparation, the bacterial culture was harvested by centrifugation at 4570 x g for 40 min at 4 °C. Plasmid purification was performed according to the Qiagen Plasmid Midi Kit (100) protocol. The DNA pellet was added 150 µl of TE buffer (Table 3.2) and left o/n at room temperature (RT) to ensure that the pellet was properly dissolved.

4.1.3 Determination of plasmid concentration and quality

After purification, the DNA concentration and quality of the plasmids were determined by optical density (OD) and agarose gel electrophoresis.

4.1.3.1 OD measurements

The absorbance of 1.0 µl solution was measured by a NanoDrop ND-1000 spectrophotometer at 260 nm to determine the plasmid concentration. The 260/280 ratio was considered to estimate the DNA purity. A ratio of approximately 1.8 indicates a pure sample as RNA and DNA absorb at 260 nm. A ratio lower than 1.8 indicates protein or phenol contamination, while a ratio higher than 1.8 can indicate RNA contamination. The 260/230 ratio should range between 2.0-2.2 to indicate a pure DNA sample. A lower ratio could indicate impurities such as phenol or guanidine residues (Thermo Fisher Scientific, 2015).

4.1.3.2 Agarose gel electrophoresis

To verify the quality of the DNA, the CEL plasmids were separated on a 1 % agarose gel. The gel contained 0.5 µg/ml ethidium bromide to visualize the DNA. Before loading the gel, a restriction digestion was set up for each plasmid using the enzyme *Bam*HI (Table 3.2). The reaction was incubated at 37 °C for 1 h and then left at 80 °C for 20 min for inactivation. Both digested and undigested plasmids (500-1000 ng) were loaded onto the gel. 10 µl sample was mixed with 2 µl of Gel Loading dye Blue (6x) before loaded adjacent to a 10 kb molecular size marker. The gel was run in 1x TBE buffer (Table 3.11) at 90 V for 2 h. The ChemiDoc MP Imaging System was used for visualization.

Table 4.1 Restriction digestion with *Bam*HI

Reagents	Amount
Plasmid DNA	1 µg
10X CutSmart Buffer	5 µl
*Bam*HI	1 µl
dH_2O	43 µl
Total volume	50 µl

4.2 Cell culturing, transfection and treatment of cells

4.2.1 Cell culturing

Mouse pancreatic acinar cells, 266-6 (ATCC) and human embryonic kidney cells, HEK-293 (CloneTech) were cultured in Dulbeccos Modified Eagle's Medium (DMEM) with high glucose (4500 mg/ml) supplemented with 10 % fetal bovine serum and 100 U/ml Antibiotics Antimycotic. The cells were grown in a humidified atmosphere with 5 % CO_2 at 37 °C in T75 cm^2 flasks if not stated otherwise.

4.2.2 Passaging and seeding of cells

Sub-culturing was done by removing the growth medium and washing the cells with 3 ml pre-warmed PBS. Next, 1 ml 0.05 % Trypsin-EDTA was added for the cells to detach from the surface. Subsequently the cells were resuspended in growth media and an appropriate dilution of cells was transferred to a new T75 cm^2 flask and added a total of 13 ml growth media. For experiments that required an exact number of cells, an aliquot of the resuspended cells (5 µl)

were diluted 1:100 in PBS before counted using a Scepter 2.0 cell counter or a Countess II Automated Cell Counter following the manufacturer's protocol.

4.2.3 Cell freezing and thawing

Cells were grown to 80-90 % confluency in a T75 cm^2 flask prior to freezing. The cells were in log phase growth when freezing to ensure recovery and optimum health when thawed (ATCC, 2010). The cells were trypsinized as described above (section 4.2.2) and transferred to a 15 ml Falcon tube before centrifuged at 1000 x g for 4 min. The supernatant was removed, and the pellet resuspended in 5 ml freezing medium (10 % DMSO in complete growth medium). The cell suspension was aliquoted in cryo vials and placed in a container with isopropanol at -80 °C. After 72 h, the vials were transferred to a nitrogen tank for long-term storage.

Rapid thawing of cells is important to avoid DMSO to destroy the cell membrane (Baboo et al., 2019). A cryo vial containing 1 ml of cells were thawed by rubbing between palms, resuspended in 5 ml pre-warmed complete growth medium and transferred to a T25 cm2 flask. The next day, medium was removed, and cells were added fresh growth medium to remove debris and DMSO residue.

4.2.4 Transient transfection of 266-6 cells by nucleofection

Prior to transfection, cells were grown to 70-80 % confluency in T75-flasks. Also, 72 h before transfection, 100 nM dexamethasone was added to the cells for proper differentiation of the 266-6 cells into an acinar like-phenotype (Derikx et al., 2015).

Transfection was performed using the Nucleofector 4D technology by Lonza according to the manufacturer's protocol. Nucleofection, which is a sophistical form of electroporation, uses a combination of electrical parameters and solutions that need to be optimized specifically for each cell line. The transfection protocol presented here was carefully optimized for the 266-6 cell line. An overview of the protocol is presented in Figure 4.2. In brief, cells were washed, trypsinated, resuspended in 5 ml DMEM and counted using the CellCountess II apparatus (step 1). The cells (9 x 10^6) were centrifuged at 90 x g for 10 min at RT and the supernatant was removed. The cell pellet was resuspended in transfection mix consisting of 1 µg DNA, 82 µl SF solution and 18 µl S1 supplement. The transfection mix was transferred to cuvettes and pulsed by the DN-100 program (step 3). Next, 400 µl of low-calcium RPMI media was added to cuvettes and left to incubate at 37 °C for 10 min (step 4). 2/3 of the pulsed cell suspension was transferred to one well of the 6-well plate for Western blot analysis, whereas 1/3 of the cell

suspension was transferred to one well of the 12-well plates for immunostaining and confocal analysis (step 5). The transfected cells were grown for 48 h at 37 °C before further analysis.

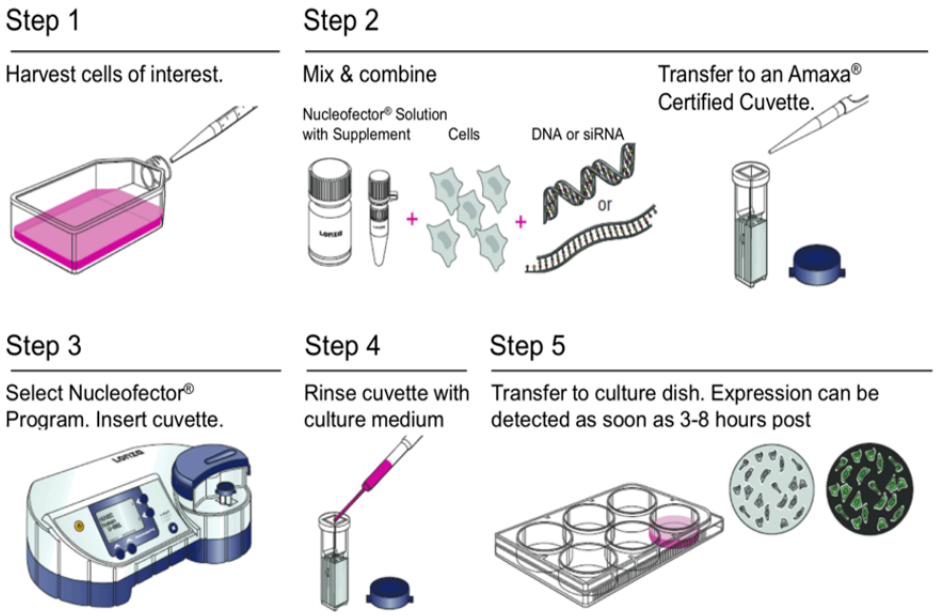

Fig 4.2 Transfection of 266-6 cells by nucleofection. Figure is taken from the Lonza 4D nucleofection protocol.

4.2.5 Transient transfection of HEK-293 cells by Lipofectamine

Prior to transfection, HEK-293 cells were seeded in a 6-well plate (4 x 10^6 cells per well) and grown to 60-70 % confluency. The transfection was executed as described by the Lipofectamine 2000 manufacturer protocol. For each transfection, 4 µg DNA was diluted in 250 µl Opti-MEM media and incubated for 5 min at RT. Similarly, 10 µl Lipofectamine was diluted in 250 µl Opti-MEM media and subsequently the DNA mix was added to the Lipofectamine mix and incubated at RT for 20 min. Next, the lipid-DNA solution was added to the cells and incubated at 37 °C. After 4-6 h, the growth medium was replaced, and the cells further incubated for 48 h before SDS-PAGE and Western blot analysis.

4.2.6 Treatment of 266-6 cells

266-6 cells were treated with cigarette smoking extract (CSE) or ethanol. According to Murty Pharmaceuticals, the CSE is made by burning University of Kentucky 3R4F standard research cigarettes on a filter smoke machine. The cigarette smoke is condensed, stored and further extracted with DMSO by soaking and sonication. The CSE is packaged as 40 mg/ml (equivalent

to 3.6 cigarettes per ml). For treatment of our cells, 4 or 40 µg/ml CSE were used as these concentrations fall within the range of light smoking (equivalent to 5 cigarettes a day) and heavy smoking (equivalent to 25 cigarettes per day), respectively. For treatment with ethanol, concentrations of 10 mM or 50 mM were used. Ethanol at 10 mM corresponds to two drinks a day while 50 mM represents alcohol consumption typical of alcoholics. The cells were added CSE or ethanol 24 h post-transfection. The cells were grown for additional 24 h before further analysis.

4.3 Preparation of cellular fractions

4.3.1 Preparation of lysate, pellet and medium fractions

Forty-eight hours post transfection analytical fractions were prepared from cells seeded in 6-well plates. From each well, one ml medium was collected and centrifuged for 5 min at 14 000 x g at 4 °C. The supernatant was transferred to a new tube and analyzed as the medium fraction. The cells were washed with 1 ml PBS and lysed in ice-cold 150 µl RIPA lysis buffer (Table 3.11). The lysate was collected by a cell scrapper and sonicated on ice for 10 s x 5 with a 10 s interval. The tube was centrifuged for 20 min at 14 0000 x g at 4 °C. The supernatant was collected and analyzed as the soluble lysate fraction. The pellet was washed in 1 ml PBS centrifuged for 5 min at 14 000 x g and 4 °C. This step was performed twice. The PBS was removed, and the pellet was added 100 µl 2 x LDS loading buffer and 5 % β-mercaptoethanol, denatured at 95 °C for 5 min and analyzed as the insoluble lysate/pellet fraction. If not used immediately, all fractions were stored at -80 °C until further analysis.

4.3.2 Determination of protein concentration

The protein concentration of the lysate fractions was determined by using the Pierce BCA Protein Assay. Between 4-20 µg of total protein was used for SDS-PAGE and Western blot analysis. For the pellet and medium fraction, the volume loaded onto the SDS gel was identical to that of the corresponding lysate.

4.4 SDS-PAGE and Western blotting

4.4.1 SDS-PAGE

For the lysate and media fractions, 20 µl samples were prepared as described in Table 4.3. Before loading the SDS-gel, the samples were denatured for 15 min at 56 °C. The insoluble pellet fractions were prepared as described above (section 4.3.1). All samples were loaded onto

10 % NuPage Bis-Tris gels (1.0 mm, 10 wells) and separated by electrophoresis in a XCell SureLock Mini-Cell system. As molecular weight markers, 2 µl of Magic Mark XP and 4 µl of Precision Plus Marker were loaded onto the gels. The gels run in a 1x 3-(N-morpholino) propanesulfonic acid (MOPS) buffer at 90 V for 15 min and then at 180 V for 1 h.

Table 4.3 Content of lysate and media fractions loaded onto the SDS-gel.

Reagents	Volume
Sample/dH_2O	12 µl
β-mercaptoethanol (14.3 M)	1 µl
Sample Buffer (x4)	2 µl
Reducing Agent (x10)	5 µl
Total volume	20 µl

4.4.2 Western blotting

After SDS-PAGE, the proteins were transferred to polyvinylidene fluoride (PVDF) membranes using the XCell Blot Module system as described by Invitrogen. Prior to transfer, the membranes were activated in 100 % methanol for 1 min, followed by 1 min rinse in dH_2O. Blotting was performed at 30 V for 1 h in 1X NuPage transfer buffer containing 10 % methanol. The membranes were blocked in 5 % milk in PBS-T (0.05 %) at RT for 1 h before incubated with primary antibodies diluted in 1% milk in PBS-T (0.05 %) o/n at 4 °C. The primary antibodies used were anti-V5 (1:10 000), anti-CEL (1:5000, St. Louis), anti-CEL (1:5000, Sigma), anti-CEL-HYB (1:300) or anti-BIP (1:5000). Also, primary antibodies against the housekeeping proteins GAPDH (1:2000) and anti-actin (1:1000) were included as loading controls. The following day, the membranes were washed 3x 5 min in PBS-T (0.05 %) before incubated with HRP-conjugated secondary antibodies diluted 1:5000 in 1 % milk PBS-T (0.05 %) for 1 h at RT. Next, the membranes were washed 1x 15 min and 3x 5 min in PBS-T (0.05 %) before developed using the Pierce ECL Plus Western Blotting Substrate kit. For detection, the ChemiDoc™ MP Imaging System was used.

4.5 Immunostaining and confocal imaging

266-6 cells were transfected by nucleofection (section 4.2.4) and seeded on coverslips coated with poly-L-lysine in 12 well plates. After 48 h, the cells were washed with pre-warm PBS (37 °C) and fixed in 500 µl of 3% paraformaldehyde for 30 min. After fixation, the cells were

washed twice with PBS followed by storage in PBS at 4°C or staining as described below. All buffers used for immunostaining are described in Table 3.11, and all incubations were performed at RT if not stated otherwise.

4.5.1 Immunostaining

Cells were incubated for 3x 5 min in washing buffer before permeabilized for 20 min. Next, the cells were washed 3x 5 min and further incubated for 30 min in blocking buffer. For primary antibody incubation, the coverslips were added 40 µl of anti-V5 (1:1000 in blocking buffer) and incubated for 2 h. Cells were washed o/n at 4 °C and incubated with Alexa Fluor 488 anti-mouse HRP-conjugated secondary antibody (1:200 in blocking buffer) for 1 h. After a second washing step o/n at 4 °C, the coverslips were rinsed in PBS before mounting onto objective slides in 10 µl of Prolong Gold Antifade solution with DAPI. The slides were set to harden o/n and then further stored at -20 °C.

4.5.2 Confocal imaging

Images were obtained using a Leica TCS SP8 STED 3x confocal microscope (Leica Microsystems) equipped with an HCX PL APO CS 100x objective (NA 1.4) using oil as immersion medium. The scan speed was set to 600 Hz and bidirectional X scanning was on. Diode 405 and Argon 488 lasers were used, and the zoom factor was set to 1.4 for all images. The microscope software LAS X was used for image acquisition.

4.6 Immunohistochemistry

Formalin Fixed Paraffin Embedded (FFPE) human or mouse pancreatic tissue sections (3-5 µm) were placed onto Klinpath slides and dried o/n at 58 °C. Slides were stored at 4 °C until further analysis. Human pancreatic tissue sections were obtained from a biobank at the Department of Clinical Medicine, University of Bergen. The biobank consists of biological material sampled from patients with pancreatic cancer and other diseases of the exocrine pancreas. The study has been approved from the Regional Ethical Committee of Western Norway (REK 2013/1772).

Before starting, the slides were incubated once more at 58 °C for 5 min. Next, the slides were deparaffinized in xylene for 2x 5 min, rehydrated with decreasing ethanol concentrations (100 %, 96 % and 80 %) for 2x 2 min each and washed in dH_2O for 1 min while shaking. All washing steps were performed while shaking. The tissue sections were further incubated with retrieval buffer in a pressure cooker at 120 °C for 1 min and cooled down with running tap water.

Sections incubated with the anti-CEL antibody (1:200, Sigma) were retrieved in Tris-EDTA buffer (pH 9.0) whereas sections incubated with the CEL-HYB antibody (5 µg/ml) were retrieved in a sodium citrate buffer (pH 6.0, Table 3.11). Sections were washed 3x 5 min with PBS-T (0.05 %) and further blocked for 30 min at RT in 10 % goat serum (Table 3.8). Next, tissues were delineated with a DAKO pen and incubated with primary antibody in a humidified chamber o/n at 4 °C.

The following day, the primary antibody was removed, and the sections were washed 3x 15 min in PBS-T (0.05 %) and blocked with 3 % endogenous peroxidase (Table 3.11) for 10 min at RT. Detection of the primary antibody was performed with MACH3 anti-rabbit kit. First, sections were incubated with the probe followed by an HRP-conjugated polymer. Both incubations was performed at RT for 20 min and washing steps of 3x 5 min was done with PBS-T (0.05 %) after each step. Visualization was done with 3,3´-diaminobenzidine (DAB) as substrate. The sections were also stained for 10 min with hematoxylin to visualize the nuclei. Finally, the sections were dehydrated in increasing ethanol concentrations (80, 96 and 100 %) 1 min each, followed by xylene for 2x 2 min. The sections were mounted in permanent mounting media and visualized using a Leica DM2000LED microscope with a LASV4.8 software.

4.7 Mice work

4.7.1 Animals

The mice were housed and bred at the Laboratory Animal Facility, Department of Clinical Medicine, University of Bergen. The mice were kept under standard conditions with a temperature of 21 °C, a humidity of 55 %, a light/dark cycle of 12 h and they were fed normal chow diet. During the experimental period, however, the animals were fed with liquid diets as described in more detailed in section 4.7.3. Only CEL-HYB1 heterozygous and control male mice were used in this study.

4.7.2 Study approval

Both animal breeding and the animal experiment were approved by the Norwegian Animal Welfare Agency (Mattilsynet) in December 2017 (FOTS IDs 13902 and 13510, respectively).

4.7.3 Rodent liquid diets

Two rodent liquid diets were used in this study, namely the Lieber-DeCarli Shake and Pour ´82 Control diet and the Lieber-DeCarli Shake and Pour ´82 Ethanol diet. Both the control and

ethanol diet were prepared every second day, and the ingredients and amount needed to prepare the diets are listed in Table 4.6. In short, dry mix was added to autoclaved tap water and mixed with and without 95 % ethanol by vigorous shaking. The two diets here were again mixed as further described in the next section. If not used immediately, the diets were stored at 4 °C o/n.

Table 4.6 Ingredients and amount needed to prepare the Lieber-DeCarli (LDC) Control and Ethanol diet

Ingredients	For 200 ml diet
LDC-Control diet:	
RT tap water (autoclaved)	172 ml
Dry mix food	45.11 g
LDC-Ethanol diet	
RT tap water (autoclaved)	178 ml
Dry mix food	26.7 g
95% ethanol	13.4 ml

4.7.4 Ethanol feeding of mice

At the start of the experiments, the mice were 29 weeks old. The mice were housed in individual cages, and the liquid diets were their only source of food and water. Furthermore, the diets were given in glass feeding tubes as shown in Figure 4.7.

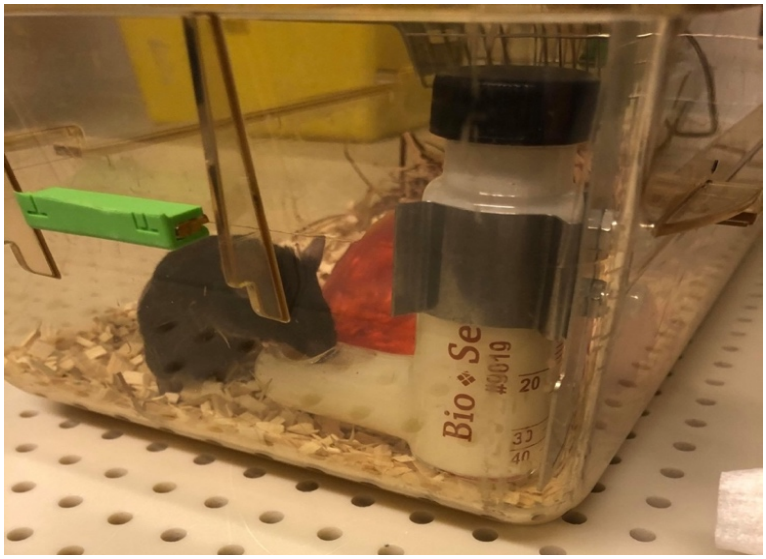

Figure 4.7: Mice fed the liquid diet. All diets were prepared as described in section 4.7.3 and were given in a glass feeding tube. An adequate amount of diets were given daily.

The mice were pair-fed meaning that one mouse was given the control diet, the other the ethanol diet. For ethanol feeding of mice, it is obligatory to introduce the alcohol gradually and to start with an adaption week (Guo et al., 2018). During the first two days, the ethanol group was fed with the control diet to get used to the liquid diet and the feeding tubes. The following days of the adaption week, the ethanol group was given an increasing amount of ethanol as shown in Figure 4.8. For the last two weeks, the mice were fed with a 5 % ethanol diet. The ethanol diet was prepared by mixing LCD-Control diet and LDC-Ethanol diet (Table 4.6) as shown in Table 4.7. The control mice were maintained on the control diet from the first to the last day of the experiment.

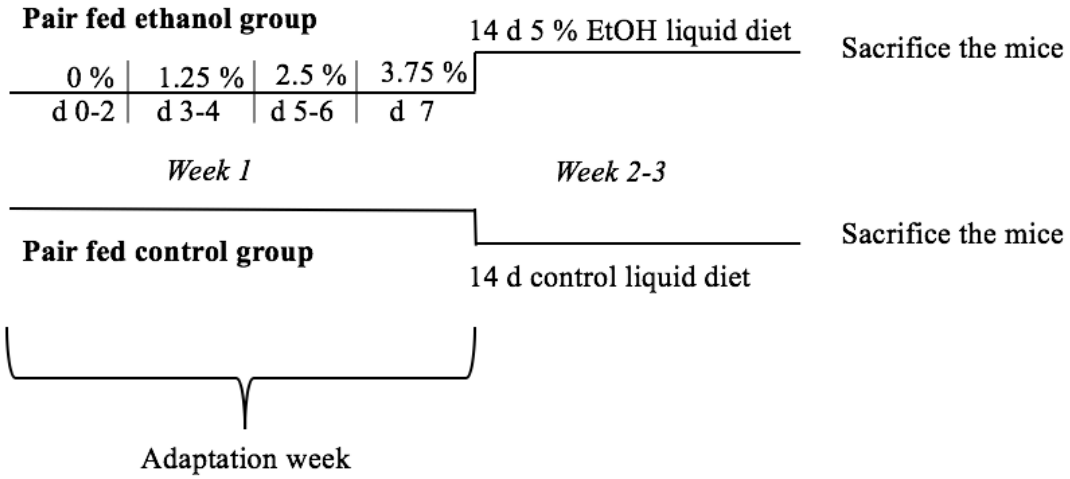

Figure 4.8 An experimental outline for ethanol and control-feeding of mice. The ethanol fed group was given an increasing percentage of ethanol in their diet for the first week before maintained at 5 % ethanol diet for the last two weeks. The control group was fed on an isocaloric adjusted control diet (see Table 4.7)

Another important principle for this experiment, is that the paired mice are fed the same amounts of calories (Guo et al., 2018). To ensure that, the food intake was measured daily (in ml) and corrected. Consequently, pair-fed mice were given the same amount of diet based on the lowest intake from the day before.

The liquid diet was changed every day between 4 and 5 pm. At the end of week 3, all mice were euthanized by CO_2. The pancreas and liver were isolated and flash-frozen on liquid nitrogen or fixed in 4 % paraformaldehyde for Western blot (section 4.4.2) and histology analysis (section 4.5.7), respectively.

Table 4.7 Isocaloric adjustment during the adaptation week with diet mixture principle

Days	Portion of LDC-Control diet (%)	Portion of LDC-Ethanol diet (%)
1-2	100	0
3-4	75	25
5-6	50	50
7	25	75
To the end of feeding	0	100

4.7.5 Histology

Pancreas tissues were fixed in 4 % formalin before paraffin-embedded sectioning (3-5 µm) was performed. The sectioning, embedding and hematoxylin-eosin staining was performed by the histology laboratory at the Department of Pathology, Haukeland University Hospital.

4.7.6 Lysis of mouse pancreatic tissue

After the mice were sacrificed, ¼ of the pancreas was cut and put in 500 µl of ice-cold 1 X RIPA buffer and placed on ice (Table 3.12). The tissue was homogenized by a pestle (ten times) before placed on a rotating wheel for 20 min at 4 ^{0}C. Next, the tissue was centrifuged at 14 000 x g for 15 min at 4 ^{0}C. The supernatant was collected and analyzed as the lysate fraction. The pellet was washed twice in 1 ml PBS and centrifuged for 5 min at 14 000 x g at 4 °C. Next, the pellet was added with 100 µl of 2x loading buffer with 2x reducing agent. The fractions were stored at -80 ^{0}C until analyzed by SDS-PAGE and Western blotting as described in section 4.4.2. Before loaded onto the SDS-gel, the pellet was incubated at 95 ^{0}C for 15 min. For the lysate, the samples loaded were prepared as described in section 4.4.1 except that no β-mercaptoethanol was added.

5. Results

5.1 Isolation of plasmids and determination of DNA quality

Plasmids encoding CEL-WT, CEL-HYB1, CEL-TRUNC or EV (empty vector) were transformed into *E.coli* bacteria and further purified by using a Qiagen Plasmid Midi Kit (sections 4.1.1 and 4.1.2, respectively). Next, OD measurements were performed to estimate DNA concentration and quality. In addition, the plasmids were analyzed by agarose gel electrophoresis to confirm purification success. The plasmids were linearized with the restriction enzyme *Bam*HI, and both cut and uncut plasmids were analyzed on the gel (Figure. 5.1). For the digested plasmids we observed the expected band sizes around 7.3 kb for CEL-WT, 7.1 kb for CEL-HYB1, 6.8 kb for CEL-TRUNC and 5.5 kb bp for EV, respectively. For all undigested plasmids, the supercoiled form of the plasmid was detected as a strong band a bit lower than the respective linearized sample. In addition, a very weak upper band was seen that most likely represent open circular forms of the plasmids. Taken together, these results confirmed that the plasmids were intact and of good quality.

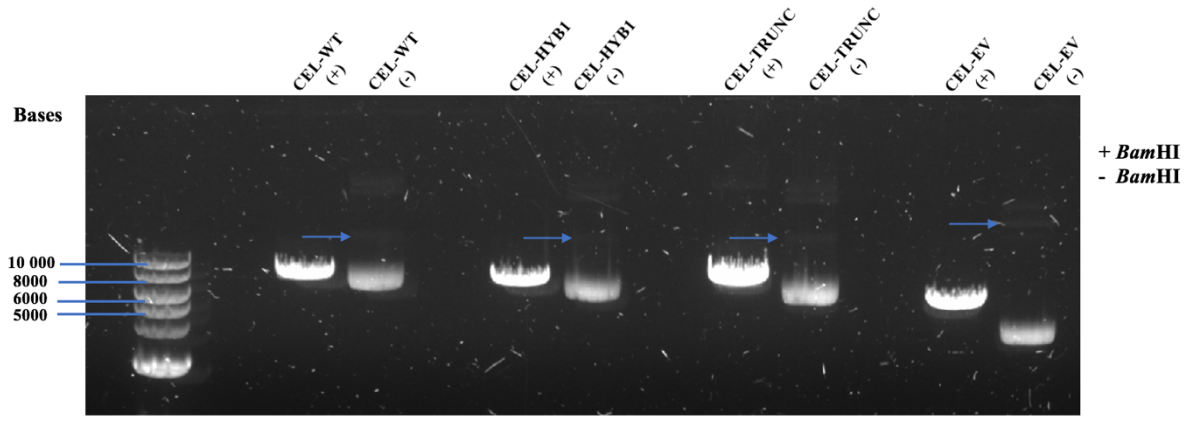

Figure 5.1 Verification of plasmids by agarose gel electrophoresis. Plasmids (500-1000 ng) were loaded and separated on a 1 % agarose gel before stained with ethidium bromide. The plasmids were linearized with *Bam*HI and digested/undigested plasmids are indicated with (+)/(-), respectively. Arrows point to weak bands that may correspond to open circular plasmids of undigested samples.

5.2 Protein structure of CEL variants

The plasmids used in this study are encoding different CEL variants, and a schematic overview of these proteins is presented in Figure 5.2. For CEL-WT, we used the variant with 16 VNTR repeats, which is the most common CEL protein in the general population. In addition to CEL-WT and CEL-HYB1, we included an artificial CEL variant; CEL-TRUNC. This variant only

harbors the first four amino acids of the first VNTR. This variant was included as a control to study the biological effect of an absent VNTR region

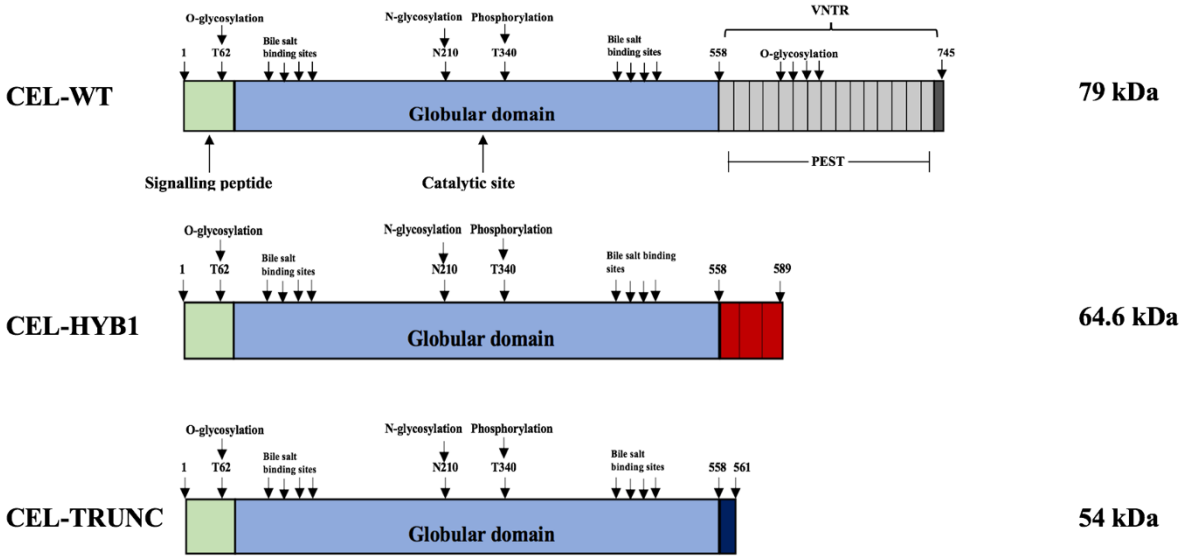

Figure 5.2. Schematic overview of CEL protein variants employed in this study. CEL protein variants are presented with their functional domains and sites, theoretical size (kDa) and VNTR length indicated. All variants share identical signaling peptide (green) and globular domain (blue). The CEL-WT protein has 16 VNTR repeats (grey), CEL-HYB1 has three VNTR repeats (red) whereas CEL-TRUNC lacks the VNTR region expect for four amino acids of the first repeat (dark blue). Drawn after: Fjeld et al., 2015. *Nat Genet* and Johansson et al., 2018. *Pancreatology.*

5.3 Expression of CEL protein variants in cell model systems

All functional studies on the CEL-HYB1 protein has been performed using non-pancreatic human HEK-293 cells by our group (Fjeld et al., 2015, Tjora et al., unpublished). Now, we wanted to use the 266-6, which is a mouse acinar cell model, to study the CEL-HYB1 protein in a more suitable environment. Previous attempts to use the 266-6 cells have proven difficult using transfection by Lipofectamine as the transfection efficiency was only ~20 %. We therefore set out to try nucleofection as a new transfection approach.

5.3.1 Optimization of cell transfection using nucleofection

For optimization, 266-6 cells were transiently transfected with a vector encoding green fluorescent protein (GFP). GFP is often used as a reporter to determine transfection efficiency (Zizzi et al., 2010) and the percentage of cells expressing GFP in a population can be determined

by microscopy. Different amounts of cells were seeded to determine optimal transfection efficiency for immunofluorescence (IF) and Western blot (WB) experiments (section 4.5.1 and 4.4.2, respectively). Forty-eight h post transfection, images were taken to determine the transfection efficiency.

For IF, cells were seeded in 12-well plates at different densities as indicated in Figure 5.3A. The best transfection efficiency was observed with 6 million cells/well. However, we decided to use 3 million cells/well to avoid confluent cells for proper staining and visualization. For WB, cells were seeded in 6-well plates (Figure 5.3B). Here, best transfection efficiency was seen for 6 or 9 million cells/well. Since 9 million cells/well showed more cell death than 6 million cells/well, the latter was used for further experiments.

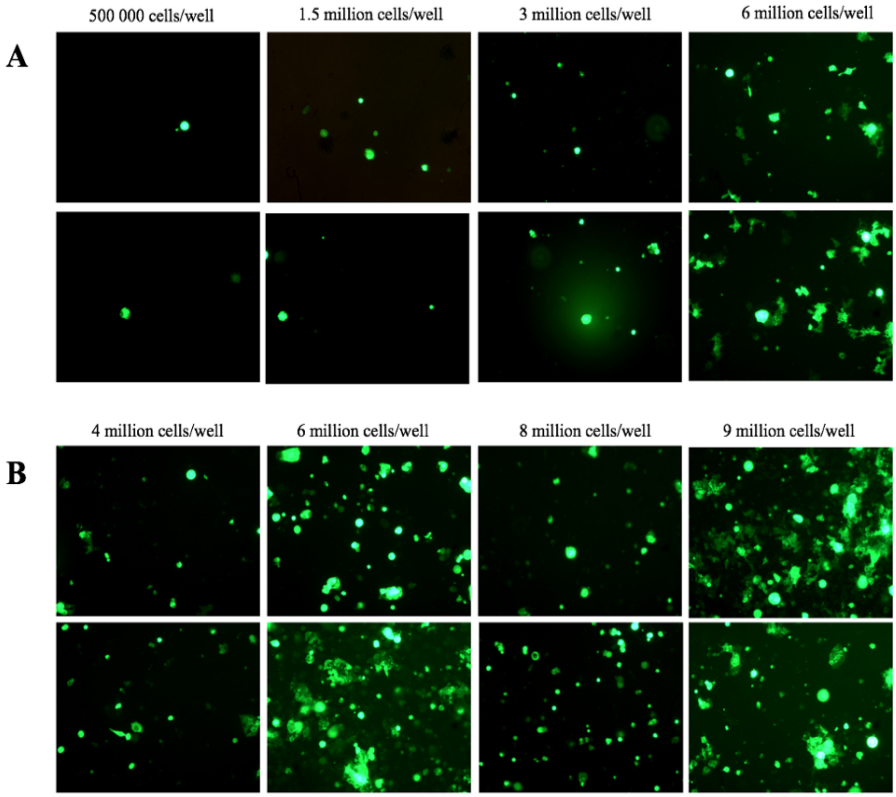

Figure 5.3 Optimization of nucleofection of 266-6 cells. A titration of different number of cells/well were performed to determine optimal transfection efficiency for 266-6 cells. The cells were transfected with a vector encoding GFP. Cells expressing GFP are seen in green. **A)** For immunofluorescence, 500,000, 1.5 million, 3 million or 6 million transfected cells were seeded per/well in 12-well plates. **B)** For Western blot, 4, 6, 8 or 9 million transfected cells were seeded per/well in 6-well plates. This experiment was conducted once.

5.3.2 Expression of CEL in 266-6 and HEK-293 cells

Once the nucleofection method was optimized for the 266-6 cells, they were transiently transfected for investigation of CEL protein expression and secretion with plasmids encoding CEL-WT, CEL-HYB1 or CEL-TRUNC. Empty vector (EV) was included as a negative control. 48 h post transfection, cell fractionation was performed for isolation and analysis of lysate, pellet and media fraction by Western blotting (section 4.3.1 and 4.4.2). Protein expression was detected by using either the anti-CEL (Sigma, cat.nr. SAB2103782) antibody or anti-CEL (St. Louis) antibody (Figure 5.4). Anti-GAPDH was used as a loading control for the lysates.

When using the CEL antibody from Sigma, only the CEL-WT protein was detected (Figure 5.3 A, left panel). This was expected since the antibody recognizes the VNTR region of the CEL-WT protein. The WT protein was observed in both the lysate and media fraction. In the media fraction, two bands were detected between 120 and 100 kDa. In the lysate fraction, one strong CEL-WT band was seen close to 100 kDa. These CEL-WT bands represent different glycosylated forms of the protein (Johansson et al., 2011, Torsvik et al., 2014). In addition, one unspecific band between 60 and 80 kDa was detected in all wells.

The Western blot results when using the anti-CEL (St. Louis) antibody are shown in Figure 5.3A (right panel). This antibody recognizes the globular domain of the CEL protein and was therefore expected to detect all CEL variants. To our surprise, however, only CEL-WT was detected here as well, in the medium and the pellet fractions.

In previous experiments done by our research group, the anti-CEL (St. Louis) antibody worked well to detected various CEL proteins including CEL-HYB1 and CEL-TRUNC by Western blotting (unpublished data). The only difference was that the expression system had been HEK-293 and not 266-6 cells which were used in the present study. To test if the lack of CEL protein detection in our study was due to the choice of cell model or a possible error in the CEL-expressing plasmids, HEK-293 cells were transiently transfected with Lipofectamine using the same constructs as described above (section 4.2.5). Western blot analysis of the three cellular fractions is shown in Figure 5.4B. Now, all CEL variants could be detected. In the media fraction, only the CEL-WT protein was detected (between 100 and 120 kDa). In the pellet fraction, however, strong bands were observed for both CEL-HYB1 (about 65 kDa) and CEL-TRUNC (about 60 kDa). In the same fraction, also a weak band was seen for the CEL-WT protein (about 80 kDa). In the lysate, a strong CEL-WT band and more faint CEL-HYB1 and

CEL-TRUNC bands were seen at similar sizes as described above. Similar to the left panel of Figure 5.4A, there were unspecific bands detected in the lysate fractions for all variants.

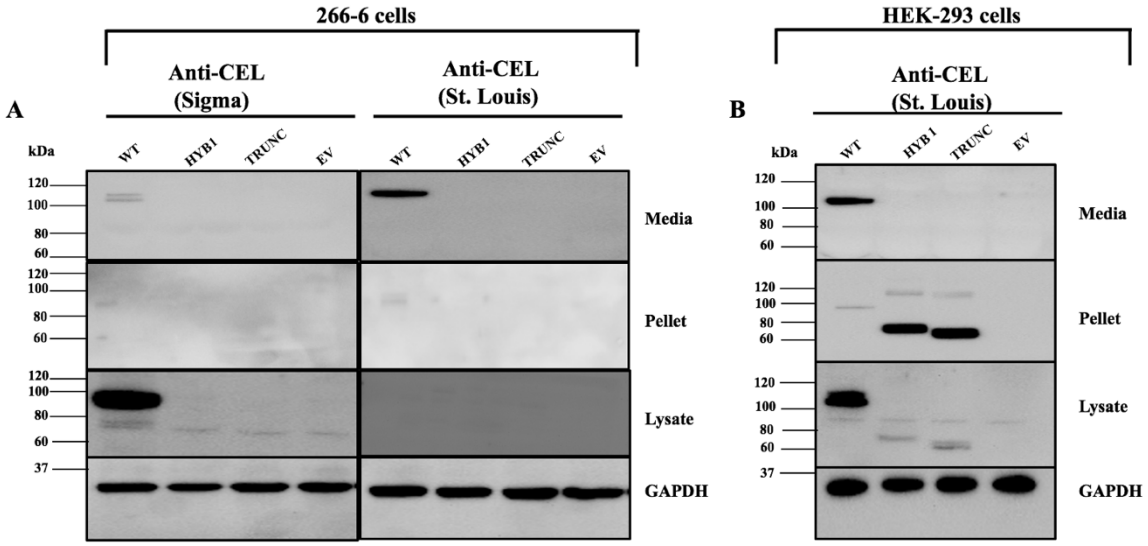

Figure 5.4. Expression of CEL in 266-6 cells and HEK-293 cells. A) The 266-6 cells were transiently transfected by nucleofection with plasmids encoding CEL-WT, CEL-HYB1, CEL-TRUNC or EV. Media, pellet and lysate fractions were analyzed by SDS-PAGE and Western blotting using an antibody that recognizes the VNTR region of the CEL-WT protein (Sigma) or an antibody that that recognizes the globular domain of the CEL protein (St. Louis). GAPDH was used as a loading control. **B)** HEK-293 cells were transiently transfected by Lipofectamine with the same plasmids as in A. Media, lysate and pellet fractions were isolated and analyzed by SDS-PAGE and Western blotting by using the anti-CEL (St. Louis) antibody and GAPDH as a loading control. This experiment was conducted one time.

Taken together, the three tested CEL variants were detected at the expected molecular size when expressed in HEK-293 cells but not 266-6 cells. This indicates that the constructs were fine, and that the differences observed was due to the choice of cell line. The CEL-HYB1 was only observed in the pellet fraction in HEK-293 cells. Further, CEL-HYB has been reported to be more insoluble in previous studies (Tjora et al., unpublished).

5.4 Expression of V5-tagged CEL variants in 266-6 cells

Since we failed to detect CEL expression in transfected 266-6 cells, we decided to change approach by transfecting the cells with V5-tagged plasmids. Our research group have made such plasmids for several CEL variants including CEL-WT, CEL-HYB1 and CEL-TRUNC, and they have all been used with success (Johansson et al., 2011, Fjeld et al., 2015). A schematic overview of the CEL protein variants encoded by the V5-tagged plasmids is presented in

Appendix 1. The V5-tag is located in the C-terminal of CEL and is attached to the protein by a linker region.

Now, we also included a second CEL-HYB1 plasmid for some of our experiments, to investigate if there was any difference in expression or intracellular distribution between the two CEL-HYB1 variants. In the new CEL-HYB1 variant (denoted CEL-HYB1^{N}, see Appendix 1), two serine residues was mutated in the linker region between the protein and the V5-tag. These two residues were introduced into the original CEL-HYB1 construct by accident (Fjeld et al., 2015), and since they could introduce an extra N-glycosylation they were now changed to alanine and glycine, respectively. Thus, CEL-HYB1^{N} was included in this study to investigate the effect of the potential N-glycosylation site introduced to the C-terminal of CEL-HYB1

5.4.1 Western blot analysis of different CEL protein variants in 266-6 cells

The 266-6 cells were nucleofected and fractionated 48 h post transfection as previously described. The cell fractions were isolated and analyzed by Western blotting using an anti-V5 antibody and GAPDH as loading control.

Figure 5.5 displays the Western blot analysis of V5-tagged CEL variants. In the media and lysate fractions, CEL-WT and CEL-HYB1 proteins were detected. In addition, a faint CEL-TRUNC band was observed in the media fraction. Furthermore, unspecific signals were seen in the media and could be IgG heavy chain bands at around 50 kDa. Only the CEL-HYB1 protein was observed in the insoluble pellet fraction indicating that this variant is less soluble than the normal protein also when expressed in acinar cell.

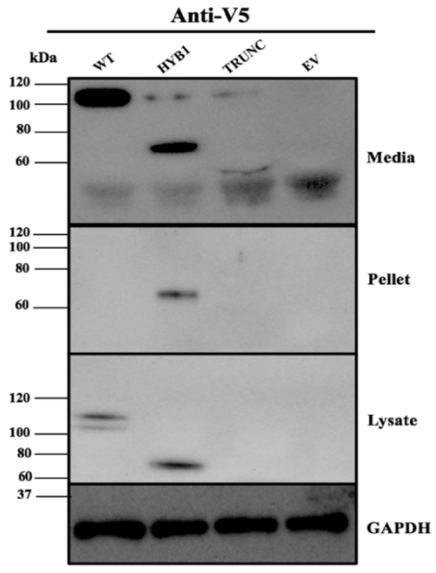

Figure 5.5 Expression of different CEL protein variants in 266-6 cells. The 266-6 cells were nucleofected with plasmids encoding CEL-WT, CEL-HYB1, CEL-TRUNC or EV containing a V5-tag. Media, pellet and lysate fractions were analyzed by SDS-PAGE and Western blot using an anti-V5 antibody. As a loading control GAPDH was used. The figure is representative for three individual experiments.

Based on these results, we decided to use the V5-tagged plasmids for transfection of 266-6 cell throughout this master project.

5.4.2 Immunofluorescence and confocal analysis of 266-6 cells

To further investigate how the CEL protein variants distributes in the 266-6 cells, immunofluorescence and confocal imaging was performed on transiently transfected cells. The cells were fixed and stained 48 h after transfection and CEL proteins were detected by using an anti-V5 primary antibody and the secondary antibody Alexa Fluor 488 (green). DAPI was used to visualize the nuclei. (section 4.5.1 and 4.5.2.)

In this experiment, the cells were transfected with plasmids encoding CEL-WT, CEL-HYB1, CEL-TRUNC and EV. In addition, the CEL-HYB1^{N} variant was included to investigate if there was a difference between the two CEL-HYB1 variants.

Confocal images of the immunostainings are presented in Figure 5.6. Interestingly, we saw that many of the cells clustered together to form acini-like structures. For the CEL-WT expressing cells, the protein was weakly detected within the lumen of such an acinus. A similar expression pattern was observed for both CEL-HYB1 variants, however with much stronger signals. Furthermore, CEL-HYB1 showed a more intense signal than the CEL-HYB1^{N} variant. The CEL-TRUNC variant displayed a different expression pattern than the other variants. Here, less signals were observed, and the protein formed small clusters close to the nuclei.

Interestingly, more cell death was observed for the CEL-HYB1 variant than for the CEL-WT, CEL-TRUNC and the CEL-HYB1^{N} variant. The transfection efficiency, in all three experiments, were considered to be low, especially for the CEL-TRUNC variant (~ 10 % transfection efficiency).

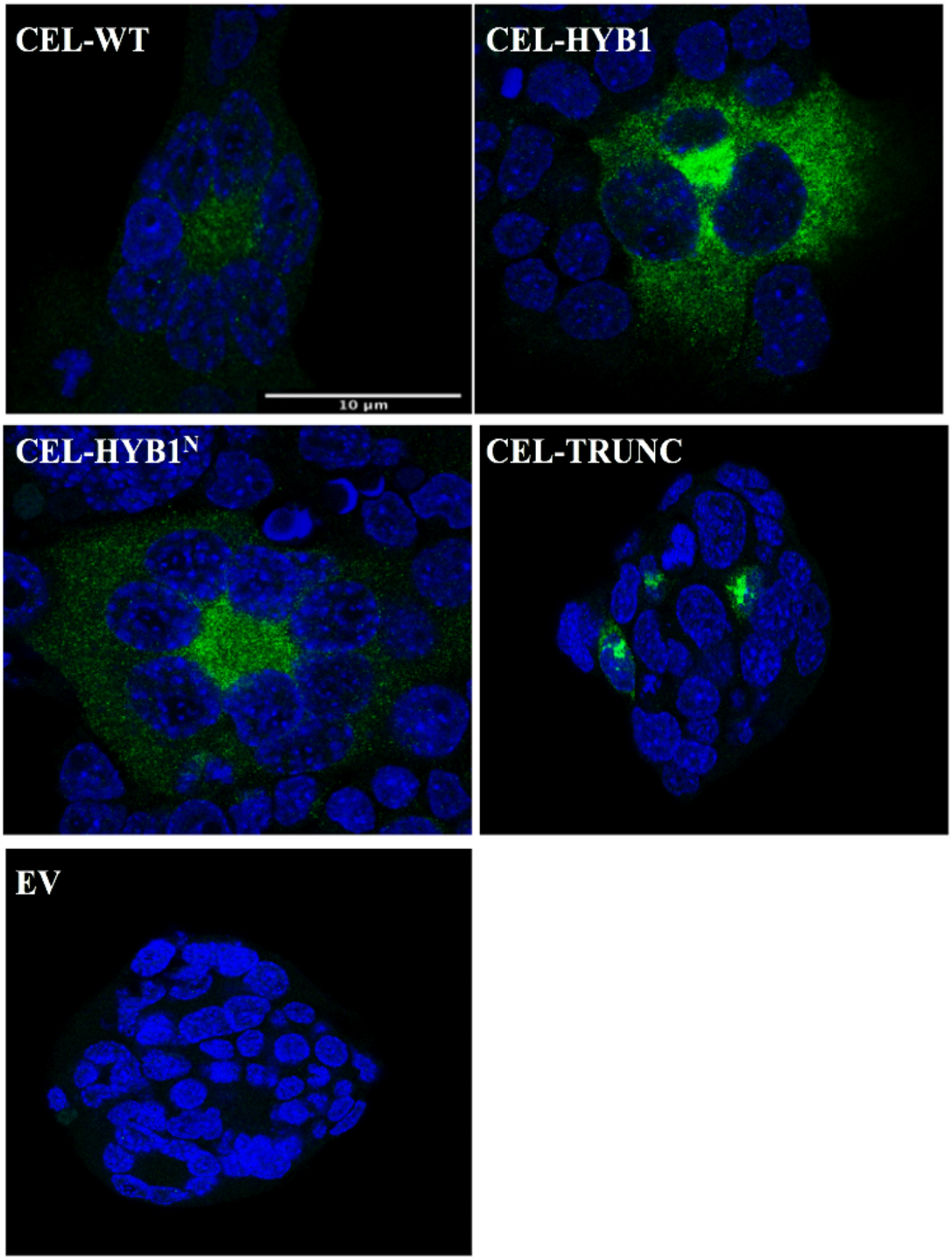

Figure 5.6 Intracellular distribution of CEL variants in 266-6 cells. Transiently transfected 266-6 cells expressing different CEL variants were fixed and stained 48 h post transfection using an anti-V5 antibody followed by a secondary antibody (Alexa Fluor 488, green) for detection. DAPI was used to visualize the cell nuclei (blue). Cells were analyzed by a Leica SP8 confocal microscope at 100x magnification. The scale bar is set to 10 µm. The figure is representative for three individual experiments.

5.5 The impact of ethanol and cigarette smoke extract on CEL-HYB1 protein expression

To investigate the effect of CEL-HYB1 in combination with environmental factors, we exposed acinar 266-6 cells to ethanol (EtOH) and smoke extract (CSE). Dexamethasone treated 266-6 cells were nucleofected with plasmids encoding CEL-WT, CEL-HYB1, CEL-TRUNC, CEL-HYB1^{N} and EV (section 4.1.1). Twenty-four h post transfection, the cells were treated with low or high doses of CSE (4 and 40 µg/ml) or ethanol (10 and 50 mM), respectively. The cells were incubated for additional 24 h, fractionated into lysate, pellet and media fractions and analyzed by Western blotting (section 4.2.4. and 4.4.). As controls, untreated cells and/or cells treated with DMSO (equal to 40 µg/ml CSE) were used.

Figure 5.7 shows the Western blot analysis of cells treated with CSE. For the control panel, one strong CEL-WT band and two weaker bands for CEL-HYB1 and CEL-HYB1^{N}, respectively, were observed in the media fraction. In the pellet, only the CEL-HYB1 variant was detected. The CEL-HYB1^{N} was not observed which could be due to an air bubble. In the lysate fraction, all CEL variants were detected.

For the DMSO treated cells, the CEL-WT variant showed a strong band in the media and a fainter signal in the lysate fraction. For the CEL-HYB1 variants, they were only observed in the pellet. As for CEL-TRUNC, it was not detected at all.

The cells exposed to low dose of CSE (4 µg/ml) showed a similar expression pattern as the cells treated with DMSO, except that the CEL-HYB1^{N} had a stronger band than CEL-HYB1 in the pellet. In contrast, cells exposed to 40 µg/ml CSE showed CEL-WT, CEL-HYB1 and CEL-HYB1^{N} in the media fraction. In the lysate fraction, all variants were detected, and in the pellet fraction the CEL-HYB1 and CEL-HYB1^{N} variants were observed more intense bands.

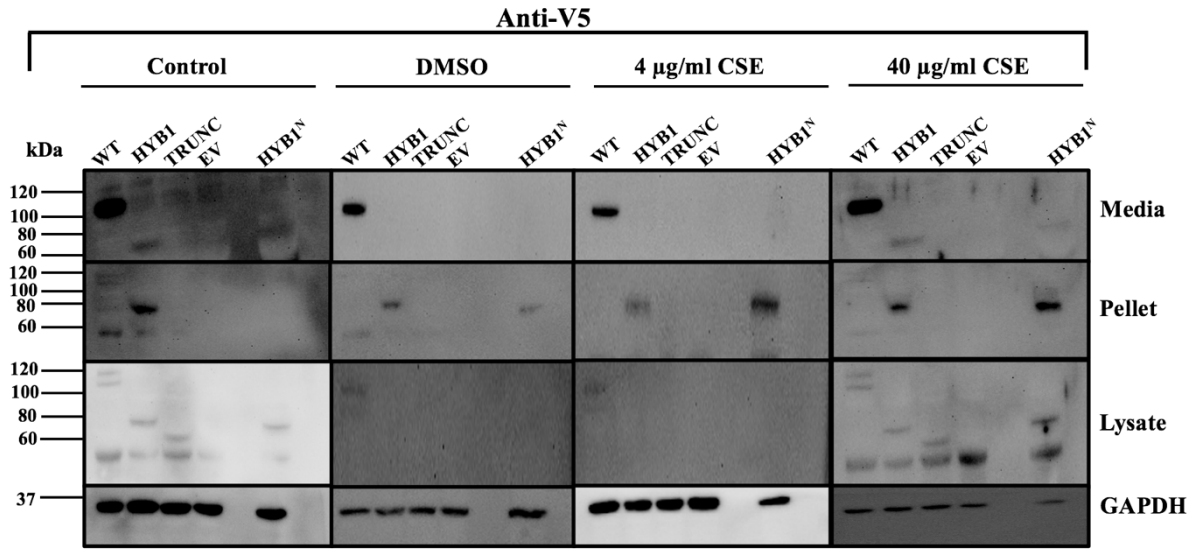

Figure 5.7 The effect of CSE on CEL protein variants. Dexamethasone treated 266-6 cells were transfected with V5-tagged constructs encoding CEL-WT, CEL-HYB1, CEL-HYB1^{N}, CEL-TRUNC or EV. Twenty-four h post transfection, cells were exposed to 4 or 40 µg/ml CSE for 24 h. As controls, untreated and DMSO treated cells were used. The cells were fractionated into media, pellet and lysate fractions and analyzed by SDS-PAGE and Western blotting using an antibody that recognizes the V5-tag. Anti-GAPDH antibody was used for loading control. The experiment was performed once.

The effect of ethanol on CEL variants is shown in Figure 5.8. The control panel displayed different patterns compared to the control panel for CSE treated cells (Figure 5.7). Here, only the CEL-WT was observed in the media while CEL-HYB1^{N} and a faint CEL-HYB1 band were seen in the pellet fraction. In the lysate fraction, none of the variants were detected.

The same expression pattern was observed in the cells exposed to 10 mM EtOH. After treatment with 50 mM EtOH, however, none of the variants were observed in the media and lysate fractions. Weak bands of CEL-HYB1 and CEL-HYB1^{N} were observed in the pellet fraction whereas CEL-TRUNC was not detected in any fractions during this experiment.

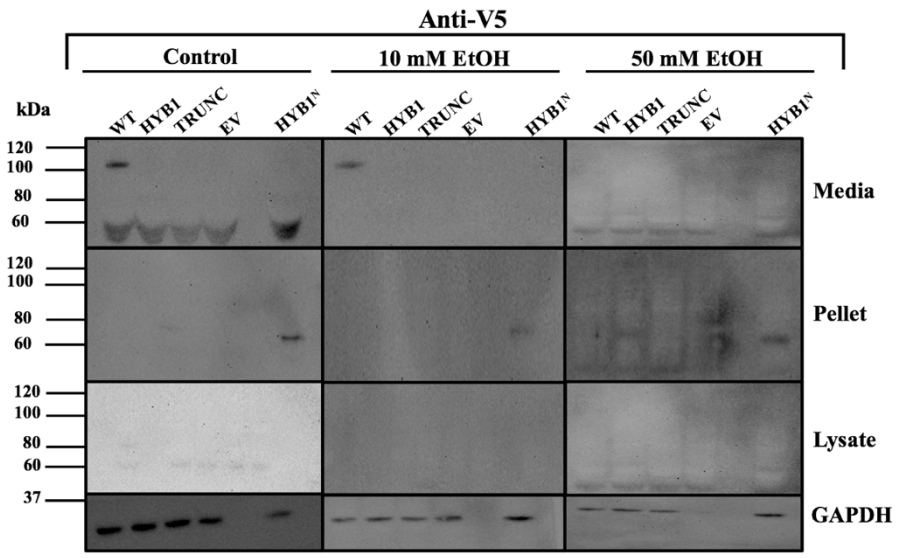

Figure 5.8 The effect of EtOH on CEL protein variants. The 266-6 cells were transfected with V5-tagged constructs encoding CEL-WT, CEL-HYB1, CEL-HYB1^{N}, CEL-TRUNC or EV. Twenty-four h post transfection, cells were treated with 10 or 50 mM EtOH. As a control, untreated cells were used. Twenty-four h post treatment, cells were fractionated into media, pellet and lysate fractions and analyzed by SDS-PAGE and Western blotting and detected by anti-V5 antibody. GAPDH was used as a loading control. One parallel of this experiment was conducted

In summary, the CEL-HYB1 variants tended to have stronger bands in the pellet fractions for cells treated with 4 and 40 µg/ml CSE compared to DMSO. In addition, the CEL-HYB1^{N} variant exhibited stronger bands than the CEL-HYB1 variants when exposed to CSE. This pattern was not detected for the EtOH treated cells. However, CEL-HYB1^{N} showed a stronger band than CEL-HYB1 in all pellet fractions.

5.6 The effect of ethanol on transgenic CEL-HYB *knock-in* mice

To study the effect of EtOH on transgenic CEL-HYB1 (0/ki) mice, we used 29-week-old male animals. C57BL/6N (0/0) mice were included as controls. The mice were pair-fed with control or EtOH-containing liquid diet as described in section 4.7.3. In short, after a 7-day acclimatization period (see Figure 4.8) the mice were fed a Lieber-DeCarli ethanol-containing (5 % v/v) liquid diet for 2 weeks. The pair-fed control group received an ethanol-free liquid diet for 2 weeks. The mice were sacrificed after 3-week with liquid feeding. This experiment was set up as a pilot and we included 3 pairs of mice: two controls (0/0, pair 1 and 2) and one CEL-HYB1 (0/ki, pair 3).

5.6.1 Food consumption and body weight

Average food consumption was around 20 ml when the experiment started. Then, the food intake decreased to about 15 ml when the ethanol diet was introduced and remained at this level throughout the experiment. Daily weighing showed that the control fed group gained weight during the three weeks while the EtOH fed group lost weight. (see Appendix 2 for growth curves).

5.6.2 Pancreas histology of EtOH-fed mice

After sacrificing the mice, one part of the pancreas was isolated and fixed for histological analysis (section 4.7.5.). Hematoxylin-eosin staining of pancreas sections from control- and ethanol-fed mice are shown in Figure 5.9. The histology of the pancreas in all mice, independent of diet, appeared normal. There was no sign of fibrosis or other features indicating chronic pancreatitis. The 0/ki mice fed with the control diet showed some fat in the pancreas. However, this is most likely due to body weight as this mouse was heavier than the other animals (see Appendix 1 for growth curve).

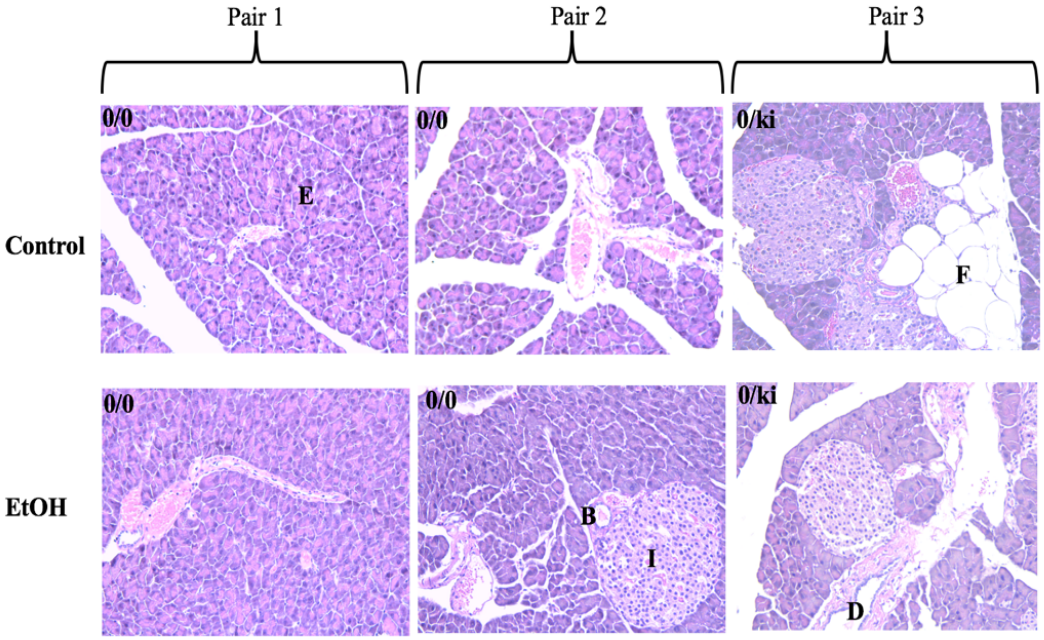

Figure 5.9 Effect of EtOH-feeding on pancreas histology. Pancreas sections from controls (0/0, pair 1 and 2) and CEL-HYB1 (0/ki, pair 3) mice were stained with hematoxylin-eosin. Upper panel: Control mice; Lower panel: EtOH treated mice. I; Islets of Langerhans, E; exocrine pancreas D; Duct, F; Fat, B; Blood vessel. All images are 20x magnification and this experiment was performed once. Control, control liquid diet; EtOH, ethanol-containing diet. The experiment was performed once.

5.6.3 CEL and BIP expression in the pancreas of ethanol-fed mice

Even though we found no signs of histological changes in the pancreas of ethanol-fed mice, we wanted to investigate if ethanol could induce cellular stress in the organ. To do so, we isolated pancreatic lysates and insoluble pellet fractions from both control and ethanol-fed mice (section 4.7.6*),* and these fractions were further analyzed by Western blotting (Figure 5.10). As a stress marker, we used an antibody towards the ER-chaperone BIP. BIP is a master regulator of the unfolded protein response and is responsible for proper folding and assembly of proteins. The predicted molecular weight of BIP is 78 kDa. In addition, we analyzed CEL expression in the mice using the anti-CEL (St. Louis) antibody.

The lysate fractions were analyzed for CEL expression. Here, we observed endogenous Cel expression in all mice at expected size around 66 kDa. The mouse Cel protein has a shorter VNTR region (only 3 repeats) and is therefore smaller in size compared to the normal human CEL protein (16 VNTR repeats). For the CEL-HYB1 mice, we observed an additional band (marked with an arrow in Figure 5.11). This corresponds to the humanized CEL-HYB1 protein at about 64 kDa.

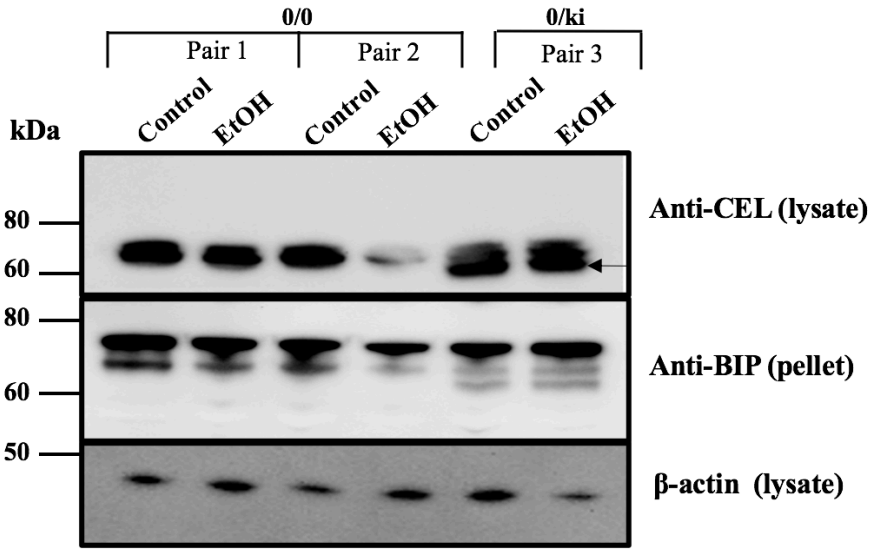

Figure 5.10. The effect of EtOH on CEL and BIP expression in the pancreas from EtOH-fed mice. Mouse pancreatic lysates and pellet fractions were analyzed by Western blotting. Both endogenous and exogenous CEL expression was detected using a CEL specific antibody (St. Louis) whereas an anti- BIP antibody was used to detect ER-stress. Anti-β-actin was used as a loading control. Arrow indicates CEL-HYB1 (64 kDa). This experiment was performed once.

The pellet fractions were analyzed for the ER stress marker BIP. A band around 80 kDa was observed for all samples, with a varying intensity. However, the introduction of EtOH exposure did not have an obvious impact on BIP or CEL protein expression compared to the untreated mice.

5.7 Testing of a new CEL-HYB specific antibody

5.7.1 The CEL-HYB antibody

The hybrid-specific antibody was designed by our research group and further developed by Davids Biotechnologie GmbH (Regensburg, Germany). The antibody is a rabbit polyclonal antibody that targets the C-terminal of the CEL-HYB1 protein. More specifically, it recognizes a 10 amino acids sequence located in the VNTR region of the protein as illustrated in Figure 5.11

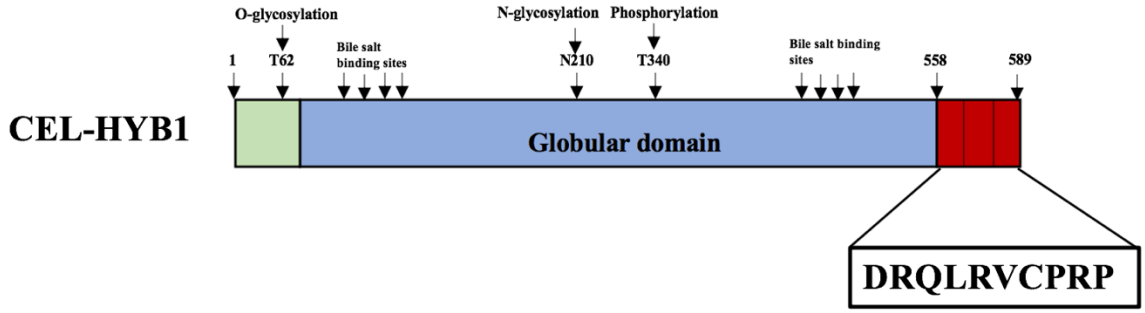

Figure 5.11 The epitope of the CEL-HYB specific antibody. The new antibody recognizes the 10 amino acid sequence DRQLRVCPRP located in the VNTR region of the CEL-HYB1 protein

5.7.2 Testing the CEL-HYB antibody on transfected HEK-293 and 266-6 cells

To test the CEL-HYB antibody on cellular models, HEK-293 and the 266-6 cells were transfected by using Lipofectamine and nucleofection, respectively. The cells were transfected with plasmids encoding V5-tagged CEL-WT, CEL-HYB1, CEL-TRUNC or EV. Forty-eight h after transfection, the cellular fractions were prepared and analyzed by Western blotting. The blots were first incubated with the CEL-HYB antibody, then stripped and incubated with either the anti-V5 or the anti-CEL (St. Louis) antibody. The expression of GAPDH was used as a loading control.

Western blots of transfected 266-6 cells are shown in Figure 5.12A. The left panel shows incubation with the CEL-HYB antibody. No signal was observed for the CEL-HYB1 protein in any of the fractions. In the right panel, the same blot incubated with the anti-V5 antibody is presented. Here, similar to Figure 5.5, all CEL variants were detected: CEL-WT, CEL-HYB1 and CEL-TRUNC in the media, CEL-HYB1 in the pellet, and CEL-WT and CEL-HYB1 in the lysate fraction.

Figure 5.12B displays the Western blots of transfected HEK-293 cells incubated with the CEL-HYB antibody (left panel) and the anti-CEL (St. Louis) antibody (right panel). In the left panel, the CEL-HYB1 protein (about 64 kDa) was observed in the pellet fraction together with a high molecular band. The same CEL-HYB1 bands were observed in the pellet fraction in the right panel, when incubating with the anti-CEL antibody. In addition, CEL-TRUNC and a lower CEL-WT band (90 kDa) were seen in the pellet fraction. In the lysate, all three variants were present but only CEL-WT were detected in the media.

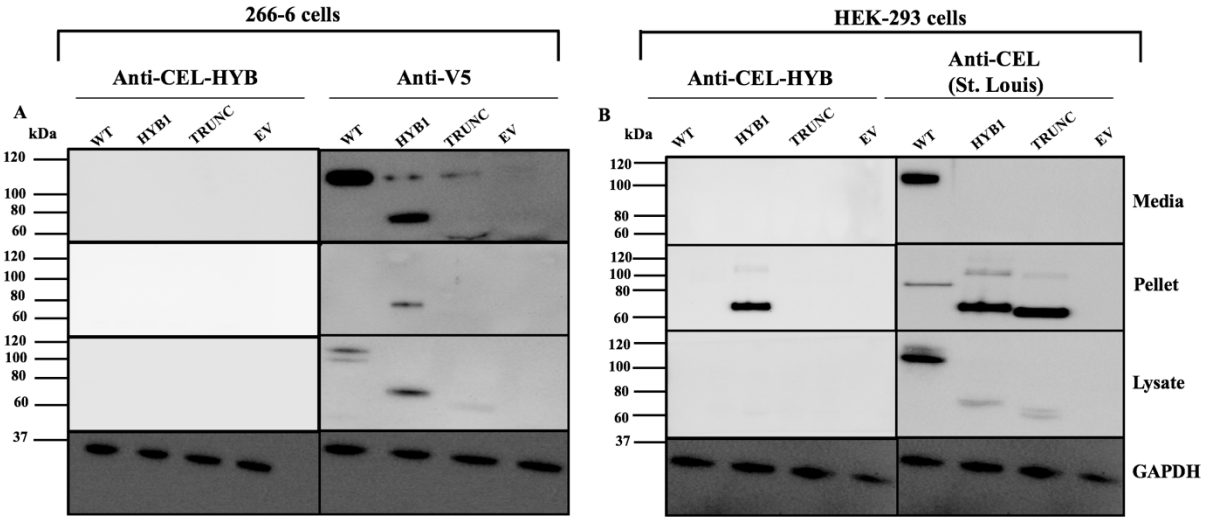

Figure 5.12 Testing the CEL-HYB antibody on transfected 266-6 and HEK-293 cells. Both cell lines were transfected with plasmids encoding V5-tagged CEL-WT, CEL-HYB1, CEL-TRUNC or EV. Cellular factions were analyzed by Western blotting and incubated with the CEL-HYB antibody, stripped and incubated with anti-V5 antibody or anti-CEL (St. Louis) antibody. GAPDH was used as a loading control. The experiment was performed once. **A)** Analysis of cellular fraction from transfected 266-6 cells using anti-HYB (left panel) and anti-V5 (right panel) antibodies. **B)** Analysis of cellular fractions from transfected HEK-293 cells using anti-HYB (left panel) and anti-CEL (St. Louis, right panel) antibodies.

Based on these results, the CEL-HYB antibody works very well for the HEK-293 cells but not the 266-6 cells.

5.7.3 Testing the CEL-HYB antibody on mouse pancreatic lysates

Next, the CEL-HYB antibody was tested on pancreatic lysates isolated from transgenic mice (section 4.7.6). Mice with different CEL genotypes were used: control mice (C57BL/6N (0/0)), heterozygous (0/ki) and homozygous (ki/ki) CEL-HYB1 *knock-in* mice (Section 3.1), and heterozygous (0/ki) 16R mice. For the latter, the mice are *knocked-in* with the 16 VNTR repeats most commonly found in the human CEL protein. The pancreatic lysates were analyzed by Western blotting. The membrane was first incubated with the CEL-HYB antibody, then stripped and incubated with the anti-CEL (St. Louis) antibody. Here, β-actin was used as loading control.

As seen in Figure 5.13, only pancreatic lysates from mice containing the CEL-HYB1 *knock-in* allele tested positive when incubated with the CEL-HYB antibody. The expected band at about 64 kDa was detected for each lysate. In contrast, when incubating with the anti-CEL antibody, all lysates displayed bands. The 0/0 mice lysates showed the endogenous Cel protein band at about 66 kDa. The heterozygous 16R mice lysates displayed two bands corresponding to the endogenous Cel protein (66 kDa) and the humanized 16R variant (100 -120 kDa). Similarly, the heterozygous CEL-HYB1 (0/ki) mice showed two bands. Here, the lower band (about 64 kDa) is the *knocked-in* CEL-HYB1 protein while the upper band (about 66 kDa) is the mouse Cel protein. The homozygous (ki/ki) mice lysates only displayed one band at about 64 kDa.

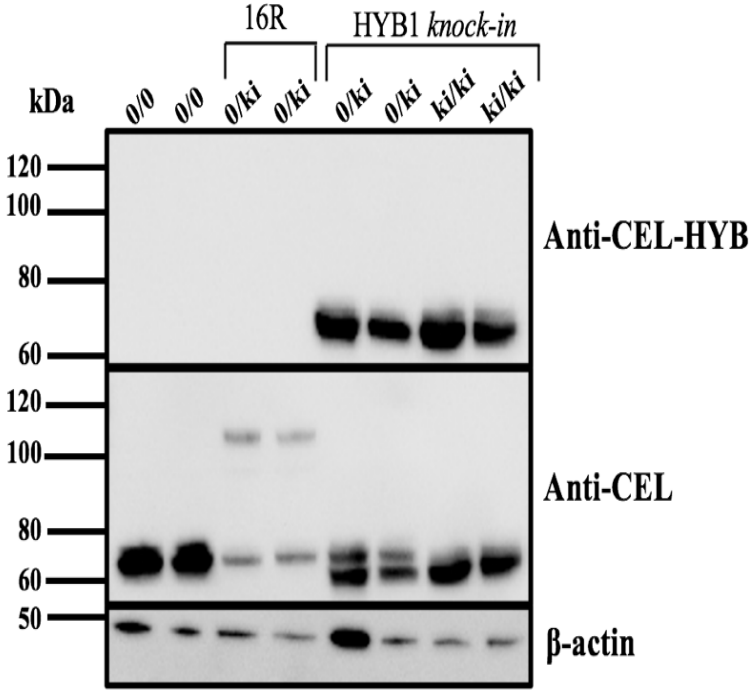

Figure 5.13 Testing the CEL-HYB antibody on mouse pancreatic lysates of different genotypes. Mice pancreatic lysates were analyzed by immunoblotting and incubated first with the hybrid-specific antibody and further with the anti-CEL (St. Louis) antibody. β-actin was used as loading control. In this experiment, lysates were obtained from control 0/0 mice, heterozygous (0/ki) and homozygous (ki/ki) CEL-HYB1 *knock-in* mice as well as the heterozygous (0/ki) *CEL-16R* mice were included. The 16R mice are transgenic mice *knocked-in* with the 16 VNTR repeats found in the human CEL protein. Only the *knock-in* CEL-HYB1 mice displayed bands when incubated with the hybrid antibody. The experiment was performed once.

Taken together, the CEL-HYB antibody worked specifically to detect the CEL-HYB1 protein only in pancreatic lysates from CEL-HYB1 transgenic mice.

5.8 Testing the CEL-HYB antibody on pancreatic tissue by immunohistochemistry

During this test, we did a range of optimization steps before ending up with the optimal conditions for the CEL-HYB antibody. Different techniques, buffers and solutions were tested to determine the optimal conditions for the antibody (see Appendix 3). Briefly, we found that a heat-induced epitope retrieval method and the sodium-citrate buffer (pH 6.0) were best suited for the antibody (see Appendix 4). In addition, a high salt-containing (150 mM NaCl) antibody diluent enhanced the staining compared to a low salt-containing (75 mM NaCl) antibody diluent (see Appendix 5).

In addition to CEL-HYB1 staining, we included staining with an anti-CEL antibody (Sigma) as a control. The protocol for CEL-staining was previously been optimized by our group (El Jellas et al., 2018). For all staining's, we used formalin fixed and paraffin embedded mouse or human pancreatic tissue.

5.8.1 Testing the CEL-HYB antibody on mouse pancreatic tissue

Figure 5.14 shows CEL-HYB and CEL staining of control mice ((C57BL/6N (0/0)) and heterozygous (0/ki) CEL-HYB1 mice. Positive staining was shown in brown while the nuclei are stained blue with hematoxylin. The anti-CEL-HYB antibody showed strong and specific staining for the 0/ki mice in the acinar cells of the CEL-HYB1 mice whereas the control mice displayed a very weak background staining in the exocrine pancreas.

As the anti-CEL antibody from Sigma recognizes amino acids within the globular domain of the protein, the antibody showed positive staining of the exocrine tissue in both 0/0 and 0/ki mice. The islets of Langerhans were negative for both antibodies, indicating that both antibodies were CEL specific since the CEL proteins are only expressed in the acinar cells of the pancreas.

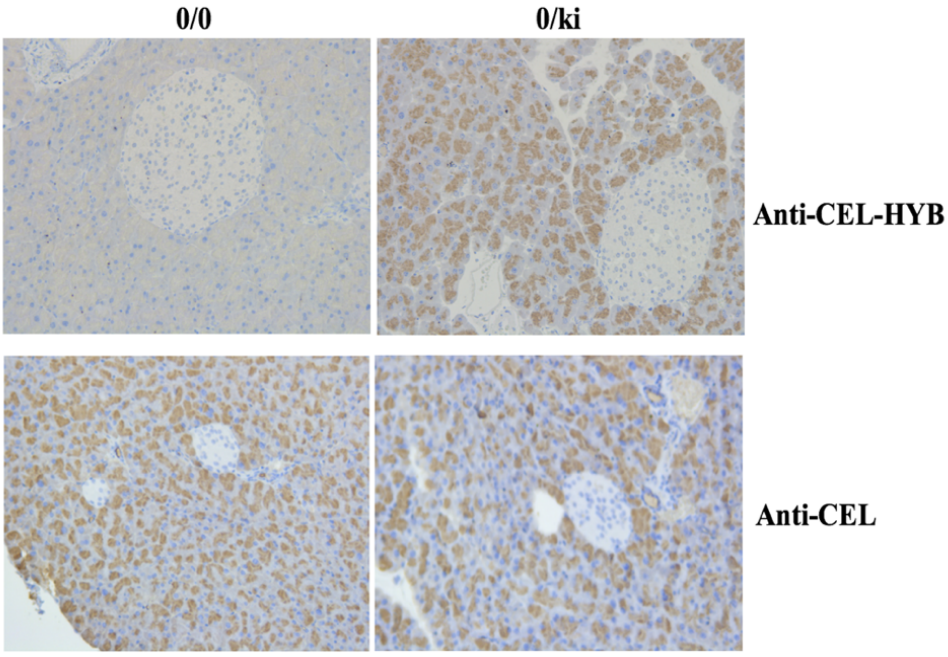

Figure 5.14. CEL staining of mouse pancreatic tissue. Pancreas sections from control (C57BL/6N (0/0)) and heterozygous (0/ki) CEL-HYB1 mice were subjected to immunohistochemistry and analyzed with the anti-CEL-HYB antibody (upper panel) or the anti-CEL (Sigma) antibody (lower panel). Images were acquired with a Leica DM2000LED microscope with a 20x magnification. The experiment was performed twice.

5.8.2 Testing the CEL-HYB antibody on human pancreatic tissue

The CEL-HYB antibody was also tested on human pancreatic tissue, using the optimized protocol developed for immunohistochemistry on pancreatic mouse tissue. Human tissue from one patient with normal pancreas and three CEL-HYB positive pancreatic cancer patients were tested.

The results are shown in Figure 5.15. Except for the control sample, all tissue showed some degree of positive staining for the CEL-HYB1 protein. Subject 1 showed a more intense and concentrated staining in the exocrine tissue than subject 2. As for the subject 3 sample, it exhibited an expression pattern similar to subject 1. The control tissue showed no positive staining for CEL-HYB1.

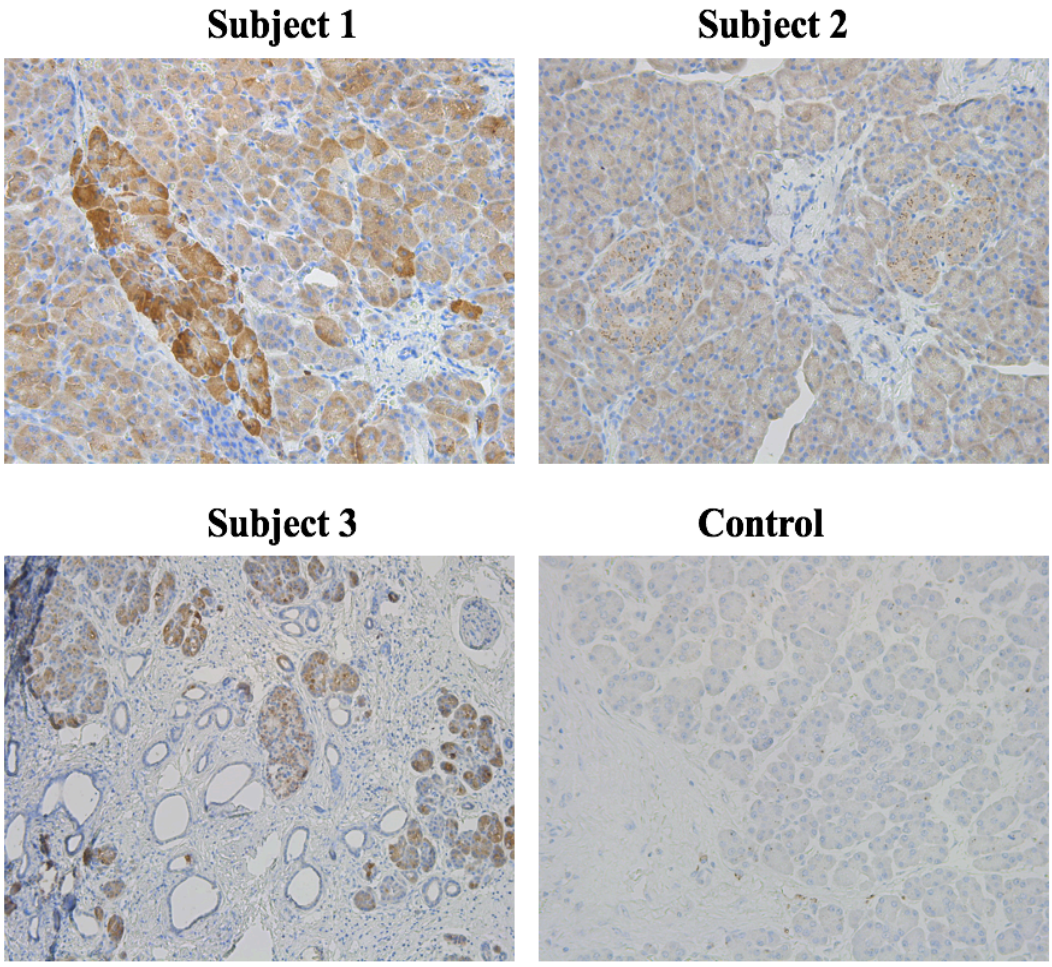

Figure 5.15. Testing the CEL-HYB antibody on human pancreatic tissue. The panel includes three samples of HYB1 positive origin and one control sample. All CEL-HYB samples showed positive staining and the control was negative. Images were acquired with a Leica DM2000 LED microscope with a 20x magnification. The experiment was performed twice.

6. Discussion

CEL-HYB1 has been identified as a genetic risk factor for chronic pancreatitis (Fjeld et al., 2015). However, a large number of healthy individuals are carrying the *CEL-HYB1* allele without being sick. Thus, *CEL-HYB1* alone is not enough to cause chronic pancreatitis; the allele must act in combination with other risk factors to trigger disease development.

In this study, our main objective was to gain more insight into the disease mechanism of the CEL-HYB1 protein. We wanted to examine if environmental factors such as alcohol and cigarette smoking could have any effects on the CEL-HYB1 protein in cellular and mouse models. In addition, a newly produced CEL-HYB1 specific antibody was tested on cellular fractions and tissue samples by immunoblotting and immunohistochemistry, respectively. The main findings and the challenges we met during this study are discussed below.

6.1 The effect of CEL-HYB1 in combination with environmental factors

6.1.1 The effect of alcohol and CSE on CEL-HYB1 in 266-6 cells

We performed one parallel of CSE and EtOH treatment of transfected 266-6 cells. We used two concentrations of CSE (4 and 40 µg/ml) and two concentrations of EtOH (10 and 50 mM), and analyzed the effect by Western blotting. The concentrations were chosen based on literature. Concentrations of 4 and 40 µg/ml corresponding to light smoking (5 cigarettes a day) and heavy smoking (25 cigarettes a day), respectively. The EtOH concentrations of 10 and 50 mM correlate with social drinking (2 glasses a day) and heavy drinking (equivalent to ethanol concentration found in alcoholics) respectively (Lee and Apte, 2015, Srinivasan et al., 2015).

First of all, when we expressed CEL-HYB1 in the 266-6 cells, we observed reduced protein secretion compared to CEL-WT, and CEL-HYB1 protein was detected in the insoluble pellet fraction (Figure 5.5). This is similar to what we see in HEK-293 cells (Fjeld et al., 2015, Tjora et al., unpublished), suggesting that the protein has a tendency to aggregate also in acinar cells. Interestingly, when exposed to CSE, the level of CEL-HYB1 increased in the pellet fractions compared to cells treated with DMSO (Figure 5.7). This may suggest that the CSE have a negative effect on CEL-HYB1, making it more prone to protein misfolding and aggregation.

Also, when exposed to CSE, the CEL-HYB1^{N} variant showed stronger bands in the pellet fractions than CEL-HYB1. This may suggest that the potential N-glycosylation site introduced to the CEL-HYB1 construct has an effect on the protein by making it more soluble. Thus, the CEL-HYB1^{N} construct should selected for further analysis.

Taken together, these results are very interesting as they indicate an interplay between CEL-HYB1 and cigarette smoking that can trigger or accelerate chronic pancreatitis disease development. However, our findings need to be replicated before we draw any conclusions. An interesting follow up study would be to investigate the downstream effects of CEL-HYB1 and CSE, e.g on ER-stress. A study has shown that the effect of CSE and alcohol in combination induces ER-stress and cell death in both AR42J cells and primary acinar cells (Lugea et al., 2017). Thus, they see an effect even without a genetic risk factor but only when the cells are exposed to both environmental factors. For additional follow up, it would be interesting to see if we could detect a link between CEL-HYB1 and cigarette smoking also in patients.

We did not observe any effect of ethanol on the CEL-HYB1 protein. However, a study conducted by Waldron *et al*, detected Cel protein aggregation and increased ER-stress in ethanol fed mice and in AR42J cells exposed to ethanol (Waldron et al., 2018). Thus, we need to repeat our experiment to investigate the effect of ethanol on CEL-HYB1. We will also use our CEL-HYB1 mouse model as further discussed below.

6.1.2 Ethanol feeding of heterozygous CEL-HYB1 *knock-in* mice

We performed a three-week pilot experiment by exposing transgenic CEL-HYB1 *knock-in* mice to ethanol. We used the 0/0 mice as controls and the mice were pair-fed for comparison. The effect of the ethanol was analyzed by harvesting the pancreas for histology and Western blot analysis.

During our pilot experiment, an article by Orekhova *et al* (Orekhova et al., 2020) was published on ethanol exposure using *CPA1* mutant mice. Like *CEL-HYB1*, this *CPA1* gene is implicated in the misfolding-dependent pathway of genetic risk in chronic pancreatitis (Mayerle et al., 2019). The *CPA1* mouse model was generated on a C57BL/6N background and they performed pair-feeding with the same Lieber-DeCarli diets as we did. However, their results differed from ours as they could clearly identify characteristics of chronic pancreatitis in their *CPA1* mice. They concluded that ethanol feeding accelerated disease progression in the ethanol fed *CPA1* mice compared control fed *CPA1* mice. A major difference between our study and Orekhova's

was that they used homozygous *CPA1* mice, while we used heterozygous *CEL-HYB* mice. In addition, they started the ethanol-feeding on mice at 5 weeks of age and the experiment lasted for 5 weeks. Orekhova *et al.* chose this early age as the pancreatic damage was minimal in the CPA1 mice at this stage and therefore the effect of ethanol could be more easily observed. In contrast, we used 29 weeks old mice and they were ethanol-feed for only three weeks.

Based on these observations, we will use younger, homozygous CEL-HYB1 mice when we plan our next experiment. In addition, we will perform ethanol feeding for a longer period to investigate if this could accelerate progression of chronic pancreatitis in our CEL-HYB *knock-in* mice.

6.2 The specificity of the new CEL-HYB antibody

The newly produced CEL-HYB antibody directed towards the HYB C-terminal peptide DRQLRVCPRP was tested for both Western blotting and immunohistochemistry. After optimizing the protocols thoroughly, we were excited to see that the antibody could recognize the CEL-HYB protein both in transfected cells, and in mouse and human pancreatic tissue.

For the human tissues, we analyzed three CEL-HYB positive patients by immunohistochemistry. Subject 1 and 2 were DNA sequenced and identified as two different CEL-HYB forms, namely CEL-HYB1 and CEL-HYB2 (Fjeld et al., 2005, Zou et al., 2016). As for subject 3, DNA sequencing could not be performed as DNA was not available.

The CEL-HYB1 sample showed strong but somewhat patchy staining in the pancreatic acinar cells (Figure 5.15). This could correlate with our observations of the HYB1 protein in transfected HEK-293 cells where it tends to accumulate within the cell (Fjeld et al., 2015). In contrast, the CEL-HYB2 sample displayed a more diffuse and even staining pattern. The *CEL-HYB2* gene has a premature stop codon in exon 10 leading to reduced protein expression due to nonsense-mediated mRNA decay (Zou et al., 2016). The observed diffuse staining pattern can therefore correspond to reduced protein expression. The last CEL-HYB sample, from subject 3, showed a strong staining pattern similar to CEL-HYB1. However, this sample needs to be DNA sequenced to get the exact genotype to distinguish between CEL-HYB1 and CEL-HYB2, although the pattern was most reminiscent of the CEL-HYB1 staining pattern.

6.3 Study limitations and challenges

6.3.1 The 266-6 cells as a model system

Our research team have previously performed cellular experiments on the CEL-HYB1 protein in HEK-293 cells (Fjeld et al., 2015, Dalva et al., 2020). These cells are a reliable tool within experimental research, as they are easy to maintain, culture and transfect as well as having a high expression level of exogenously expressed proteins (Thomas et al., 2005). Furthermore, the HEK-293 cells are of human origin which is important for proper post-translational modification of the human CEL protein (Hu et al., 2018). As a model system for pancreatic research, however, the main limitation of the HEK-293 cells is that they do not provide the proper physiological conditions as they lack the specific secretion machinery of the pancreatic acinar cells (Derikx et al., 2015).

To this date there are no commercially available human acinar cell lines. Still, alternatives of mouse and rat origin exists. Other options are to use murine and human primary murine acinar cells but these are difficult to maintain for long-term cell culture experiments and they lose their secretory characteristics easily (Blinman et al., 2000). For this project, we chose the mouse acinar cell line (266-6) as a model system to study the CEL-HYB1 protein in a more proper environment. The 266-6 cell line endogenously expresses the mouse Cel protein and other digestive enzymes (Derikx et al., 2015). Our group has previously used these cells with success for endocytosis experiments (Torsvik et al., 2014, Dalva et al., 2020), but they have proven difficult to transfect as further discussed below. Furthermore, the 266-6 cells need treatment with dexamethasone to mature their secretory characteristics (Derikx et al., 2015). So, to study the expression and secretion pattern of CEL variants in 266-6 cells, the cells were stimulated with dexamethasone both before and after transfection of CEL constructs to ensure a proper acinar cell phenotype.

In addition to the murine 266-6 cells, a rat acinar cell line (AR42J) is available that has been widely used in pancreatic research (examples are studies by Srinivasan et al., 2015, Xiao et al., 2016). The AR42J-cells have also been tested by our research group. However, they lost their acinar specific phenotype during culturing and were therefore not used for further analysis.

There are both pros and cons for most model system used in research and therefore one has to be aware of the limitations and challenges that comes with the systems. The disadvantage of using 266-6 cells for CEL related research is that the mouse Cel protein only contains 3 VNTR

repeats while the human CEL protein has 16 VNTR repeats. Therefore, translation of the human CEL protein in mouse acinar could be difficult due to differences in VNTR repeats. Furthermore, the mouse Cel protein differs from the human CEL protein with regard to post-translation modifications like O-glycosylation (Holmes and Cox, 2011).

6.3.2 Nucleofection and transfection efficiency

Previously, we have transfected the 266-6 cells with Lipofectamine, but the transfection efficiency was quite low (~20 %). Therefore, for this project, we used nucleofection as transfection method. Nucleofection is a form of electroporation that allows for direct transfer of DNA into the nucleus. We used specific solutions and the plasmid pMAX-GFP provided by the manufacturers (Lonza) to optimize the nucleofection protocol for the 266-6 cells. The results looked very promising as we observed around 80-90 % transfection efficiency (Figure 5.3). However, when transfecting the cells with our CEL constructs, analysis by immunostaining and confocal analysis revealed a transfection efficiency closer to 10-15%.

Due to the low transfection efficiency of the CEL constructs, we contacted Lonza and they provided us with some troubleshooting ideas and tips (Lonza, 2012). First, they pointed out that the vector backbone can influence the gene expression level. They had transfected two cell lines (THP-1 and HUVEC cells, respectively) and tested ten different expression vectors by conducting a luciferase expression assay, and the pcDNA3.1 vector used in this study was included. They found that the pcDNA3.1 vector displayed a very poor gene expression activity after 48 h (our conditions) while the highest expression level was observed after 4 h. Another thing to consider is the vector promoter. Our pcDNA3.1-constructs includes a CMV promoter which is a strong promoter in many mammalian cells such as HeLa and HEK-293 cells. However, the CMV promoter strength has not been tested in the 266-6 cells.

Since we do not know if the pcDNA3.1 vector backbone or promoter is appropriate for the 266-6 cells, one way to optimize our nucleofection protocol could be to use a pcDNA3.1 construct that expresses GFP. Another possibility would be to clone our CEL construct into another vector with properties better suited for the 266-6 cells. Yet another way to improve transfection efficiency is to use another approach. Viral transfection has been successfully performed using the rat AR42J acinar cells and might be the most optimal transfection method also for the 266-6 cells (Szmola and Sahin-Toth., 2010, Xiao et al., 2016).

6.3.3 The use of epitope tagged proteins

Epitope tags fused with recombinant proteins are widely used and they are great research tools. Epitope tags allow for the detection of a target protein and can be used in methods such as immunoblotting, immunofluorescence and immunoprecipitation. Moreover, some tags are traceable by live-imaging allowing for *in vivo* localization of proteins (Lodish et al., 2013). A number of tags are available with different sizes and properties, and they can be coupled to the C-terminal or the N-terminal end of the protein depending on the protein`s function (Palmer et al., 2004). Unfortunately, the use of tags can also influence the experimental results and be a study limitation. The tags can alter the chemical properties of the protein of interest and thus the results obtained can either be under-or-overestimated (Booth et al., 2018).

A study performed by our research team compared the expression of CEL protein variants with and without a C-terminal V5-tag in HEK-293 cells (Gravdal et al., unpublished). Here, the disease-causing CEL-MODY protein showed increased solubility and secretion when expressed with the tag compared to untagged CEL-MODY, which had a stronger tendency to form intracellular protein aggregates. Thus, the CEL-MODY variant showed a stronger pathogenic effect when expressed without the tag (Gravdal et al., unpublished). In another study, detection of CEL variants in the media fraction was found to be difficult when CEL was expressed with a C-terminal FLAG-tag (Dalva et al., 2020).

Based on the observations above, we set out to analyze our CEL proteins variants without an epitope tag in this study. However, when expressed in 266-6 cells, only the CEL-WT protein was detected by Western blotting. CEL-HYB1 and CEL-TRUNC were not observed in any of the cellular fractions (Figure 5.4A). In contrast, signals for all three CEL variants were detected in HEK-293 cells transfected with the same untagged CEL-construct (Figure 5.4B). Consequently, we ended up by using V5-tagged CEL constructs also for the 266-6 cells. With this approach we were able to detect all CEL variants by Western blotting (Figure 5.5) and immunofluorescence (Figure 5.6). This is most likely due to the V5-tag making the CEL proteins more soluble and/or the V5-tag is easily available for the anti-V5 antibody to recognize the protein.

6.3.4 Cell fractionation

Another explanation why the CEL-HYB1 protein was not detected in the 266-6 cells could be due to our cell fractionation protocol. A research team in St. Louis kindly provided us with a protocol for cell fractionation which have proven successful for the rat acinar cell line (AR42J).

However, the protocol did not work well on the mouse acinar cell line as we only detected the CEL-WT variant. An optimal cell fractionation protocol is therefore needed to detect all CEL variants in 266-6 cells by immunoblotting. One more thing, the CEL-HYB1 protein is known to be implicated in the misfolding-dependent pathway and possibly aggregates inside the cell (Fjeld et al., 2015, Tjora et al., unpublished, Mayerle et al., 2019). Therefore, the antibody may not be able to bind to the epitope when expressed in the acinar cells.

6.4 How the COVID-19 pandemic had an impact on my master project

In spring 2020, the spread of the COVID-19 virus led to a worldwide pandemic and this virus had a great impact on the every-day life of most people. However, with the necessary restrictions put on us by the Norwegian Government, the infection was brought under control.

For students at the University of Bergen, the restrictions involved a temporary lockdown of all laboratory work. The lockdown lasted for 6 weeks and consequently some of the experiments planned for this thesis were not performed. This mainly relates to the cellular effect of CSE and EtOH on CEL-HYB1. In this thesis, the results from only one experiment was presented (Figure 5.7 and 5.8). Cellular fractions from two additional parallels were prepared but not analyzed due to lack of time. The plan was to conduct three parallels and to present the results with quantification data. With only one experiment, no strong conclusions can be drawn.

7. Conclusions

The main purpose of this study was to gain knowledge into the disease mechanism of the pathogenic CEL-HYB1 variant, a novel risk factor for chronic pancreatitis. Based on the findings the following conclusions can be drawn:

- A protocol for successful transfection of 266-6 cells by nucleofection is established

- The CEL-HYB antibody has been verified on mouse pancreatic lysates and on HEK-293 lysates by immunoblotting

- Optimization of the newly produced CEL-HYB specific antibody on mouse and human pancreatic tissue by immunohistochemistry has been conducted successfully

- CSE treated CEL-HYB1^{N} variant showed a higher propensity to accumulate in the insoluble pellet fraction when expressed in 266-6 cells compared to the CEL-WT protein

8. Future perspectives

To gain more knowledge about CEL-HYB1, and to follow up on the results from this study, we will focus on the experiments listed below

- Further optimize the transfection efficiency/cellular fractionation protocol of the 266-6 cells

- Repeat the study on ethanol and cigarette smoking extract exposure of CEL-HYB1 transfected 266-6 cells

- Set up a new experiment for ethanol-feeding of transgenic CEL-HYB1 *knock-in* mice using younger as well as homozygous CEL-HYB1 mice, and the exposure to ethanol will be extended from three to five weeks

- Test the CEL-HYB antibody for immunofluorescence analysis

- Determine the genotype (*CEL-HYB1* or *CEL-HYB2*) of the human sample (subject 3) by DNA sequencing

References

ABOUKALI N, MAS E, BRUNEA N, BENAJIBA A, LOMBARDO D. Bile salt-dependent lipase biosynthesis in rat pancreatic AR 4-2 J cells. Essential requirement of N-linked oligosaccharide for secretion and expression of a fully active enzymes. 1993. *J Biol Chem.* 268(34):25755-63

AGHDASSI, A.A., MAYERLE J., CHRISTOCHOWITZ S. et al. Animal models for investigating chronic pancreatitis. 2011. *Fibrogenesis Tissue Repair*, 4, p. 26

ALBERTS B., JOHNSON A., LEWIS J., MORGAN D., RAFF M., ROBERTS K., WALTER P. 2015. Molecular Biology of The Cell. Sixth Edition. Garland Science.

AMERICAN DIABETES ASSOCIATION.. *Diabetes Care.* 2010 Jan; 33 Suppl 1():S62-9.

ATCC. Cryogenic storage of animal cells. [Online]. ATCC. Available: https://www.atcc.org/~/media/PDFs/Technical%20Bulletins/tb03.ashx. [Accessed 14.04.20].

BABOO J., KILBRIDE P., DELAHEYE M., MILNE S., FONSECA F., BLANCO M., et al. The impact of varying cooling and thawing rates on the quality of cryopreserved human peripheral blood t cells. 2019. *Sci. Rep*. 9:3417. 10.1038/s41598-019-39957-x

BARDEESY, N., DEPINHO, R. Pancreatic cancer biology and genetics. 2002 *Nat Rev Cancer* 2, 897–909

BOOTH WT, SCHLACHTER CR, POTE D, et al. Impact of an N-terminal Polyhistidine Tag on Protein Thermal Stability 2018. *ACS Omega*. 3(1):760-768.

BLACKBERG, L., ANGQUIST, K. A. & HERNELL, O. Bile-salt-stimulated lipase in human milk: evidence for its synthesis in the lactating mammary gland. 1987 *FEBS Lett,* 217**,** 3741.

BRAY F, FERLAY J, SOERJOMATARAM I., SIEGEL RL, TORRE LA, JAMAL A. Global cancer statistics GLOBOCAN estimates of incidence and mortality worldwide for 36 cancer in 185 countries. 2018 *CA Cancer J Clin.* 68(6):394-424

BRUNEAU N, LOMBARDO D. Chaperone function of a Grp 94-related protein for folding and transport of the pancreatic bile salt-dependent lipase. 1995. *J Biol Chem.* 233(1)209-18.

BRUNEAU N, NGANGA A, FISHER EA, LOMBARDO D. O-glycosylation of C-terminal tandem-repeated sequences regulates the secretion of rat pancreatic bile salt-dependent lipase. 1997 *J Biol Chem.* 272(43):34593-605

CAGLAR, V. , KUMRAL, B. , UYGUR, R. , AlKOC, O. , OZEN, O. and DEMIREL, H. Study of Volume, Weight and Size of Normal Pancreas, Spleen and Kidney in Adults Autopsies. 2014. *Forensic Medicine and Anatomy Research*, 2, 63-69. Doi

CHATILA AT, BILAL M, GUTURU P. Evaluation and management of acute pancreatitis. 2019. *World J. Clin. Cases*, 7, 1006–1020

CNOP M, TOIVONEN S, IGOILLO-ESTEVE M, SALPEA P. 2017. Endoplasmic reticulum stress and eIF2alpha phosphorylation: the Achilles heel of pancreatic beta cells. 2017. *Molecular Metabolism* 1024–1039.

DA SILVA XAVIER G. The cells of the islets of Langerhans. 2018. *J Clin Med*. 7:54.

DALVA, M., JELLAS, K. E., STEINE, S. J., JOHANSSON, B. B., RINGDAL, M., TORSVIK, J., IMMERVOLL, H., HOEM, D., LAEMMERHIRT, F., SIMON, P., LERCH, M. M., JOHANSSON, S., NJØLSTAD, P. R., WEISS, F. U., FJELD, K. & MOLVEN, A. 2016. Copy number variants and VNTR length polymorphisms of the carboxyl-ester lipase (CEL) gene as risk factors in pancreatic cancer. *In:* KG JEBSEN CENTER FOR DIABETES RESEARCH, D. O. C. S., UNIVERSITY OF BERGEN (ed.).

DALVA M, *et al*. Pathogenic Carboxyl Ester Lipase (CEL) Variants Interact with the Normal CEL Protein in Pancreatic Cells. 2020 *Cells* 18;9(1)

DE JACO A., COMOLETTI D., DUBI N., CAMP S., TAYLOR P. Processing of cholinesterase-like alpha/beta-hydrolase fold proteins: Alterations associated with congenital disorders. 2012 *Protein Pept. Lett.* 19:173–179. doi: 10.2174/092986612799080103

DERIKZ MH, GEISZ A, KERESZTURI E, SAHIN-TOTH M. Functional significance of *SPINK1*promoter variants in chronic pancreatitis. 2015. *Am J Physiol Gastrointest* Liver Physiol. 308:G779–G784.

EL JELLAS K, JOHANSSON B.B, FJELD K, ANTONOPOULOS A, IMMERVOLL H, CHOI H. M, HOEM D, LOWE M. E, LOMBARDO D, NJOLSTAD P. R et al. The mucinous domain of pancreatic carboxyl-ester lipase (CEL) contains core 1/core 1 O-glycans that can be modified by ABO blood group determinants. 2018. *J. Biol. Chem.* 293, pp. 19476-19491

FJELD, K., WEISS, F. U., LASHER, D., ROSENDAHL, J., CHEN, J. M., JOHANSSON, B. B., KIRSTEN, H., RUFFERT, C., MASSON, E., STEINE, S. J., BUGERT, P., CNOP, M., GRUTZMANN, R., MAYERLE, J., MOSSNER, J., RINGDAL, M., SCHULZ, H. U., SENDLER, M., SIMON, P., SZTROMWASSER, P., TORSVIK, J., SCHOLZ, M., TJORA, E., FEREC, C., WITT, H., LERCH, M. M., NJOLSTAD, P. R., JOHANSSON, S. & MOLVEN, A. 2015. A recombined allele of the lipase gene CEL and its pseudogene CELP confers susceptibility to chronic pancreatitis. *Nat Genet,* 47**,** 518- 22.

FJELD, K., BEER, S., JOHNSTONE, M., ZIMMER, C., MOSSNER, J., RUFFERT, C., KREHAN, M., ZAPF, C., NJOLSTAD, P. R., JOHANSSON, S., BUGERT, P., MIYAJIMA, F., LILOGLOU, T., BROWN, L. J., WINN, S. A., DAVIES, K., LATAWIEC, D., GUNSON, B. K., CRIDDLE, D. N., PIRMOHAMED, M., GRUTZMANN, R., MICHL, P., GREENHALF, W., MOLVEN, A., SUTTON, R. & ROSENDAHL, J. 2016. Length of Variable Numbers of Tandem Repeats in the Carboxyl Ester Lipase (CEL) Gene May Confer Susceptibility to Alcoholic Liver Cirrhosis but Not Alcoholic Chronic Pancreatitis. *PLoS One,* 11**,** e0165567.

FORSMARK C.E, VEGE S.S, WILCOX C.M. Acute pancreatitis. 2016. *N. Engl. J. Med.,* 375(20) pp. 1972-198

FOROUHI GN, NICHOLAS J, WARHAM JN. Epidemiology of diabetes. 2014. *Medicine* (Abingdon). 42(12):698–702.

GARDNER TB., ADLER DG., FORSMARK CE., SAUER BG., TAYLOR JR., WHITCOMB DC. ACG Clinical Guideline: Chronic pancreatitis. 2020. *Am J Gastroenterology.* 115(3): 322.339

GEISZ, A., SAHIN-TOTH, M. A preclinical model of chronic pancreatitis driven by trypsinogen autoactivation. 2018. *Nat Commun* 9, 5033

GRAVDAL, A., XIAO, X., CNOP, M., EL JELLAS, K., NJØLSTAD, P.R., LOWE, M. E., JOHANSSON, B.B., MOLVEN, A., FJELD, K., The VNTR in pancreatic disease: the position of single-base deletions in *carboxyl ester lipase* determines proteotoxicity. Unpublished.

GUO, F.; ZHENG, K.; BENEDE-UBIETO, R.; CUBERO, F.J.; NEVZOROVA, Y.A. The Lieber-De Carli diet-a flagship model for experimental alcoholic liver disease (ALD). 2018. *Alcohol Clin. Exp. Res.* 42, 1828–1840.

HEGYI E, SAHIN-TOTH M. Genetic risk in chronic pancreatitis: the trypsin-dependent pathway 2017. *Dig Dis Sci.* 62(7):1692–1701

HIDALDO M, CASCINU S, KLEEFF J, LABIANCA R, LOHR JM, Neoptolemos J, Real FX, et al. Addressing the challenges of pancreatic cancer: future directions for improving out- comes. 2015. *Pancreatology*. 15(1):8-18.

HOLMES, R. S. & COX, L. A. Comparative Structures and Evolution of Vertebrate Carboxyl Ester Lipase (CEL) Genes and Proteins with a Major Role in Reverse Cholesterol Transport. 2011. *Cholesterol,*

HOLTSBERG, F. W., OZGUR, L. E., GARSETTI, D. E., MYERS, J., EGAN, R. W. & CLARK, M. A. Presence in human eosinophils of a lysophospholipase similar to that found in the pancreas. 1995. *The Biochemical journal,* 309**,** 141-144.

HU, J.; HAN, J.; LI H.; ZHANG, X.; LIU L.; CHEN, F.; ZENG, B. Human embryonic kidney 293 cells: A vehicle for biopharmaceutical manufacturing, structural biology, and electrophysiology. 2018 *Cells Tissues Organs 205*, 1–8

ISHIGURO H., YAMAMOTO A., NAKAKUKI M., YI L., ISHIGURO M., YAMAGUCHI M., *et al* Physiology and pathophysiology of bicarbonate secretion by pancreatic duct epithelium. 2012. *Nagoya J. Med. Sci* 74 1.18

JOHANSSON, B. B., TORSVIK, J., BJØRKHAUG, L., VESTERHUS, M., RAGVIN, A., TJORA, E., FJELD, K., HOEM, D., JOHANSSON, S., RÆDER, H., LINDQUIST, S., HERNELL, O., CNOP, M., SARASTE, J., FLATMARK, T., MOLVEN, M. & NJØLSTAD, P. R. Diabetes and Pancreatic Exocrine Dysfunction Due to Mutations in the Carboxyl Ester Lipase Gene-Maturity Onset Diabetes of the Young (CEL-MODY). A protein misfolding disease. 2011 *The Journal of Biological Chemistry,* 286**,** 34593-34605.

JOHANSSON, B. B., FJELD, K., EL JELLAS, K., GRAVDAL, A., DALVA, M., TJORA, E., RÆDER, H., KULKARNI, R. N., JOHANSSON, S., NJØLSTAD, P. R. & MOLVEN, A. 2018. The role of the carboxyl ester lipase (CEL) gene in pancreatic disease. *Pancreatology,* 18, 12-19

KAHANOVITZ L, SLUSS PM, RUSSELL SJ. Type 1 diabetes: A clinical perspective. 2017. *Point Care*. 16:37–40.

KHARROUBI AT, DARWISH HM. Diabetes mellitus: the epidemic of the century. 2015. *World J Diabetes.* 6(6):850

KLEEFF J., WHITCOMB D.C., SHIMOEGAWA T., ESPOSITO I., LERCH M.M., GRESS T, *et al.* Chronic pancreatitis. 2017. *Nat Rev Dis Primers,* 3, p. 17060

KODVAWALA, A., GHERING, A. B., DAVIDSON, W. S. & HUI, D. Y. Carboxyl ester lipase expression in macrophages increases cholesteryl ester accumulation and promotes atherosclerosis. 2005. *J Biol Chem,* 280**,** 38592-8.

KOLAR MJ, KAMAT SS, PARSONS WH, HOMAN EA, MAHER T, PERONI OD, et al. Branched fatty acid esters of hydroxy fatty acids are preferred substrates of the MODY8 protein carboxyl ester lipase. 2016. *Biochemistry.* 55(33):4636-41.

KUMAR, ABBAS & ASTER 2013. Robbins Basic Pathology, Canada, Elsevier Saunders.

LARUSCH J, WHITCOMB DC. Genetics of pancreatitis. 2011. *Curr Opin Gastroenterol.* 27(5):467–474.

LEE AT, XU Z, POTHULA SP, PATEL MB, PIROLA RC, WILSON JS, APTE MV. Alcohol and cigarette smoke components activate human pancreatic stellated cells: implications for the progression of chronic pancreatitis. 2015. *Alcohol Clin. Exp Res.* 39:2132-2133

LERCH, M.M., GORELICK, F.S. Models of acute and chronic pancreatitis. 2013. *Gastroenterology*, 144 pp. 1180-1193

LEW, D, AFGHANI E, PANDOL S. Chronic pancreatitis: Current status and challenges for prevention and treatment. 2013. *Dig Dis Sci* 62 (7): 1702-1712

LI, F. & HUI, D. Y. Synthesis and secretion of the pancreatic-type carboxyl ester lipase by human endothelial cells. 1998. *Biochem J,* 329 (Pt 3)**,** 675-9

LIDBERG, U., NILSSON, J., STROMBERG, K., STENMAN, G., SAHLIN, P., ENERBACK, S. & BJURSELL, G. Genomic organization, sequence analysis, and chromosomal localization of the human carboxyl ester lipase (CEL) gene and a CEL-like (CELL) gene. 1992. *Genomics,* 13**,** 630-40.

LINDQUIST S, HERNELL O. Lipid digestion and absorption in early life: an update. 2010. *Curr Opin Clin Nutr Metab Care* 13:314e20.

LODISH, H., BERK, A., KAISER, C. A., KRIEGER, M., BRETSCHER, A., PLOEGH, H., AMON, A. & SCOTT, M. P. 2013. *Molecular Cell Biology (seventh edition),* New York, W. H. Freeman and Company.

LOGSDON CD, JI B.The role of protein synthesis and digestive enzymes in acinar cell injury. 2013. *Nat Rev Gastroenetrol Hepatol* 10:362-370.

LOMBARDO, D., GUY, O. & FIGARELLA, C.Purification and characterization of a carboxyl ester hydrolase from human pancreatic juice. 1978. *Biochim Biophys Acta,* 527**,** 142-9.

LOMBARDO, D. & GUY, O. Studies on the substrate specificity of a carboxyl ester hydrolase from human pancreatic juice. II. Action on cholesterol esters and lipid-soluble vitamin esters. 1980 *Biochim Biophys Acta,* 611**,** 147-55.

LOMBARDO D, Bile salt-dependant lipase: its pathophysiological implications. 2001 *Biochim Biophys Acta*. 1533(1):1-28

LONZA. Important Vector Factors for Gene Expression. Technical References Guide. 2012 [Online]. Lonza. [Accessed 15.05.20].

LOOMES, K. M., SENIOR, H. E., WEST, P. M. & ROBERTON, A. M. Functional protective role for mucin glycosylated repetitive domains. 1999. *Eur J Biochem,* 266**,** 105-11

LOPEZ PP, KHORASANI-ZADEH A. *Anatomy, abdomen and pelvis, duodenum.* 2019. StatPearls. Treasure Island (FL): StatPearls Publishing LL.

LUGEA A., GERLOFF A., SU H.Y., XU Z., GO A., HU C., FRENCH S.W., WILSON J.S., APTE M.V., WALDRON R.T., PANDOL S.J. The combination of alcohol and cigarette smoke induces endoplasmic reticulum stress and cell death in pancreatic acinar cells. 2017. *Gastroenterology.* 153(6):1674–1686.

MARIN-PEÑALVER J. J., MARTIN-TIMON I., SEVLLANO-COLLANTES C., del CNÑIZO-GOMEZ F. J. Update on the treatment of type 2 diabetes mellitus. 2016. *World Journal of Diabetes*. 7(17):354–395.

MAYERLE J, SENDLER M, HEGYI E, BEYER G, LERCH MM, SAHIN-TOTH M. Genetics and pathophysiology of pancreatitis. 2019. *Gastroenterology.*

MOLVEN A, FJELD K, LOWE ME. Lipase genetic variants in chronic pancreatitis: when the end is wrong, all's not well. 2016. *Gastroenterology* 150:1515e8.

MORE SA, KINGSTON RL, LOOMES KM, HERNELL O, BLACKBERG L, BAKER HM et al. The structure of truncated recombinant humane bile salt-dependent lipase reveals insights into heparin binding. 2011. *J Mol Biol.* 312(3):197-211.

NICKLESS A, BAILIS JM, YOU Z. Control of gene expression through the nonsense-mediated RNA decay pathway. 2017. *Cell Biosci* 7:26

ORACZ G, KUJKO AA, FJELD K, WERTHEIM-TYSAROWSKAL K, ADAMUS-BIALEK W, STEINE SJ, et al. The hybrid allele 1 of carboxyl-ester lipase (CEL-HYB1) in Polish pediatric patients with chronic pancreatitis. 2019. *Pancreatology*. 19 (4):531-534.

OREKHOVA A, GEISZ A, SAHIN-TOTH M. Ethanol feeding accelerates pancreatitis progression in *CPA1 N256K* mice. 2020. *AJP Gastrointestinal and Liver Phsyiology,*

PALMER, E. & FREEMAN, T. Investigation into the use of C- and N-terminal GFP fusion proteins for subcellular localization studies using reverse transfection microarrays. 2004. *Comp. Funct. Genomics* 5, 342–353

PANDOL SJ. The Exocrine Pancreas, ed 2011/06/02. San Rafael, Morgan & Claypool Life Sciences.

PASQUALINI E., CAILLOL N., VALETTE A., LLOUBES R., VERINE A., LOMBARDO D. Phospohorylation of the rat pancreatic bile-salt-dependent lipase by casein kinase II is essential for secretion. 2000 *Biochem J.*, 345(Pt 1), pp. 121-128

PHAM A, FORSMARK C. Chronic pancreatitis: review and update of etiology, risk factors, and management. 2018. *F1000Res.* 7

PETROV, M.S., YADAV, D. Global epidemiology and holistic prevention of pancreatitis. 2019. *Nat Rev Gastroenterol Hepatol* 16, 175–184

RAEDER, H., JOHANSSON, S., HOLM, P. I., HALDORSEN, I. S., MAS, E., SBARRA, V., NERMOEN, I., EIDE, S. A., GREVLE, L., BJORKHAUG, L., SAGEN, J. V., AKSNES, L., SOVIK, O., LOMBARDO, D., MOLVEN, A. & NJOLSTAD, P. R. Mutations in the CEL VNTR cause a syndrome of diabetes and pancreatic exocrine dysfunction. 2006. *Nat Genet,* 38**,** 54-62

RAWLA P, SUNKARA T, GADUPUTI V. Epidemiology of pancreatic cancer: global trends, etiology and risk factors. 2019. *World J Oncol*. 10(1):10–27.

REUE, K., ZAMBAUX, J., WONG, H., LEE, G., LEETE, T. H., RONK, M., SHIVELY, J. E., STERNBY, B., BORGSTROM, B., AMEIS, D. & ET AL. cDNA cloning of carboxyl ester lipase from human pancreas reveals a unique proline-rich repeat unit. 1991. *J Lipid Res,* 32**,** 267-76.

RODER P. V., WU B., LIU Y., HAN W. Pancreatic regulation of glucose homeostasis. 2016. *Exp. Mol. Med.*

ROGERS, S., WELLS, R. & RECHSTEINER, M. Amino acid sequences common to rapidly degraded proteins: the PEST hypothesis. 1986. *Science,* 234**,** 364-8

SAHIN-TOTH M. Genetic risk in chronic pancreatitis: the misfolding-dependent pathway. 2017. *Curr. Opin. Gastroenterol.* 33:390–395

SALUJA A, DUDEJA V, DAWRA R, et al. Early intra-acinar events in pathogenesis of pancreatitis. 2019. *Gastroenterology.* 156:1979–1993

SRINIVASAN P, NABOKINA S, SAID H.M. Chronic alcohol exposure affects pancreatic acinar mitochondrial thiamin pyrophosphate uptake: studies with mouse 266-6 cell line and primary cells. 2015. *Am J Phsyiol Gastrointest Liver Physiol,* 309, pp. G750-G758

SZMOLA, R. & SAHIN-TOTH, M. Pancreatitis-associated chymotrypsinogen C (CTRC) mutant elicits endoplasmic reticulum stress in pancreatic acinar cells. 2010. *Gut,* 59**,** 365-72.

TAYLOR, A. K., ZAMBAUX, J. L., KLISAK, I., MOHANDAS, T., SPARKES, R. S., SCHOTZ, M. C. & LUSIS, A. J. Carboxyl ester lipase: a highly polymorphic locus on human chromosome 9qter. 1991. *Genomics,* 10**,** 425-31

THERMO FISCHER SCIENTIFIC. *Assessment of Nucleic Acid Purity.* [Online]. Thermo Fisher Scientific. Available: https://tools.thermofisher.com/content/sfs/brochures/TN52646-E-0215M-NucleicAcid.pdf [Accessed 14.04.20].

TERZYAN, S., WANG, C. S., DOWNS, D., HUNTER, B. & ZHANG, X. C. Crystal structure of the catalytic domain of human bile salt activated lipase. 2000. *Protein Sci,* 9**,** 1783-90.

THOMAS , P., SMART, T.G. HEK293 cell line: a vehicle for expression of recombinant proteins. 2005. *J. Pharmacol. Toxicol. Methods*. 51, 187-200

TJORA, E., GRAVDAL, A., ENGJOM, T., CNOP, M., JOHANSSON, B. B., DIMCEVSKI, G.G., MOLVEN, A., FJELD, K,. Protein misfolding in combination with other risk factors in CEL-HYB1-mediated chronic pancreatitis. Under revision: EJGH.

TORSVIK, J., JOHANSSON, S., JOHANSEN, A., EK, J., MINTON, J., RAEDER, H., ELLARD, S., HATTERSLEY, A., PEDERSEN, O., HANSEN, T., MOLVEN, A. & NJOLSTAD, P. R. Mutations in the VNTR of the carboxyl-ester lipase gene (CEL) are a rare cause of monogenic diabetes. 2010. *Hum Genet,* 127**,** 55-64.

VINCENT A, HERMAN J, SCHULICK R, HRUBAN RH, GOGGINS M. Pancreatic cancer 2011. *Lancet.* 378:607–20.

WALDRON R.T., SU H.-Y., PIPLANI H., CAPRI J., COHN W., WHITLEGGE J.P., FAULL K.F., SAKKIAH S., ABROL R., YANG W., ZHOU B., FREEMAN M.R., PANDOL S.J., LUHEA A. Ethanol Induced Disordering of Pancreatic Acinar Cell Endoplasmic Reticulum: An ER Stress/Defective Unfolded Protein Response Model. 2018. *Cell Mol Gastroenterol Hepatol*. 5:479–497

WHITCOMB, D. C. Clinical practice. Acute pancreatitis. 2006. *N. Engl. J Med*. 354, 2142-50

WHITCOMB, D.C., LOWE, M.E. Human Pancreatic Digestive Enzymes. 2007. *Dig Dis Sci* 52, 1–17.

WHITCOMB, D. C. Genetic risk factors for pancreatic disorders. 2013. *Gastroenterology,* 144**,** 1292-302.

WORLD HEALTH ORGANIZATION. *Diabetes*. [Online] World Health Organization. Available from: https://www.who.int/health-topics/diabetes#tab=tab_1 [Accessed 10.03.20]

XIAO, X. *et al*. A carboxyl ester lipase (CEL) mutant causes chronic pancreatitis by forming intracellular aggregates that activate apoptosis. 2016. *J. Biol. Chem.* 291, 23224–23236

YADAV D, LOWENFELS AB. The epidemiology of pancreatitis and pancreatic cancer. 2013. *Gastroenterology*. 144:1252–1261

YADAV D, HAWES RH, BRAND RE, ANDERSON MA, MONEY ME, BANKS PA, BISHOP MD, BAILLIE J, SHERMAN S, DISARIO J. Alcohol consumption, cigarette smoking, and the risk of recurrent acute and chronic pancreatitis. 2009. *Arch Intern Med*. 169(11):1035–1045.

ZHAO JB, LIAO DH, NISSEN TD. Animal models of pancreatitis: can it be translated to human pain study? 2013. *World J Gastroenterol.* 19:7222–7230

ZIZZI A, MINARDI D, CIAVATTINI A, GIANTOMASSI F, MONTIRONI R, MUZZONIGRO G, et al. Green fluorescent protein as indication of nonviral transient transfection efficiency in endometrial and testicular biopsies. 2010. *Microsci. Red. Tech*., 73 (3), pp. 229-233

ZOU WB, BOULLING A, MASAMUNE A, et al. No association between CEL–HYB hybrid allele and chronic pancreatitis in Asian populations. 2016. *Gastroenterology*. 150:1558–1560

Appendix

Appendix 1. CEL protein variants expressed with the V5-tag. All variants share identical signaling peptide (green) and globular domain (blue). The CEL-WT protein has 16 repeats in the VNTR region (grey), CEL-HYB1 variants has three repeats (red) and the CEL-TRUNC consists of four amino acids of the first VNTR repeat (dark blue). In contrast to CEL-HYB1, the CEL-HYB1^{N} variant has a mutated N-glycosylation site within the linker region located between the protein and the V5/His-tag. Drawn after: Fjeld et al., 2015. *Nat Genet* and Johansson et al., 2018. *Pancreatology.*

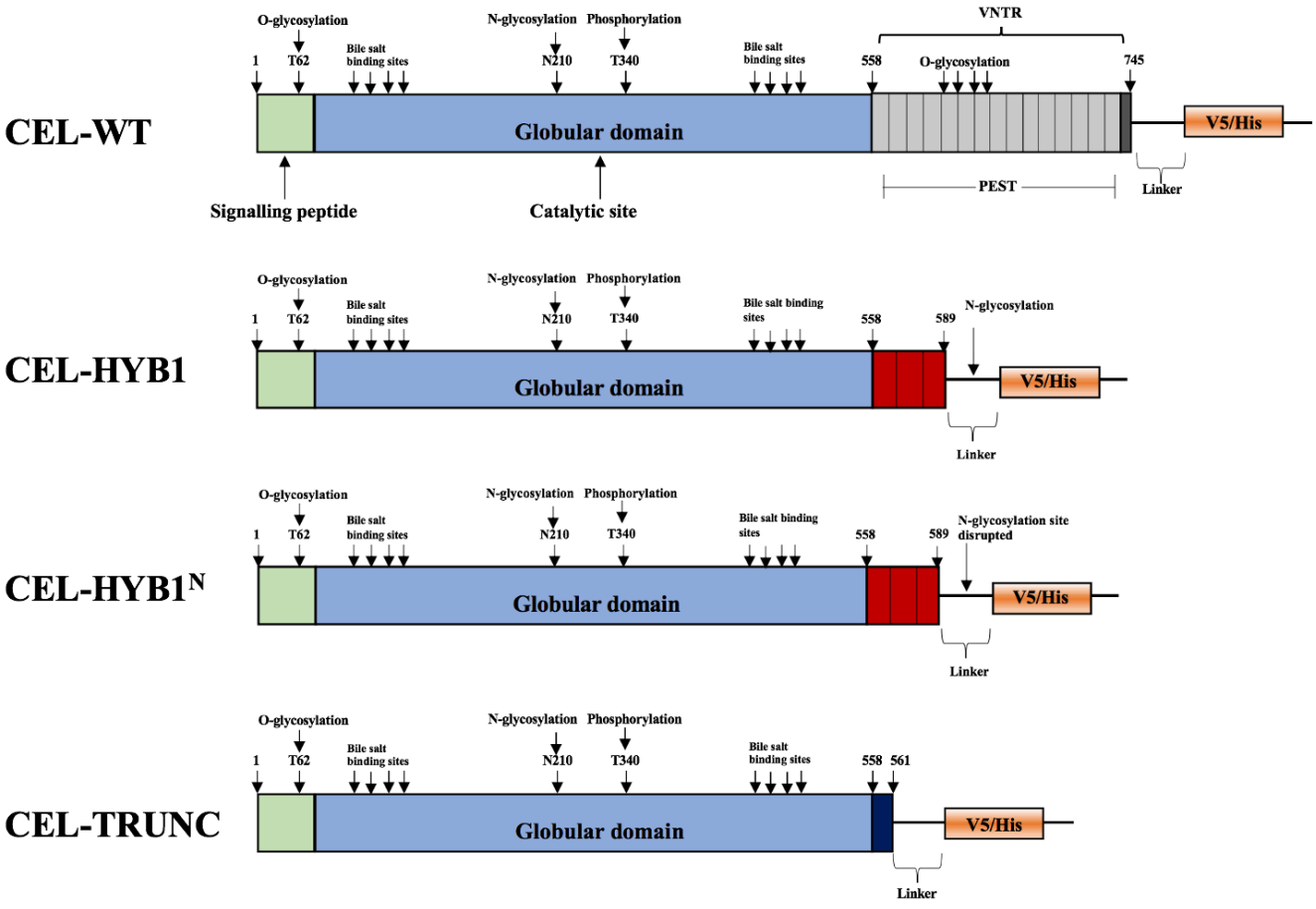

Appendix 2. Growth curves of mice fed with liquid diet. The control mice had a starting weight of 34-39 g while the heterozygous CEL-HYB1 mice had a starting weight of 39-40 g. At the end of the experiment, the control fed animals had an overall increased body weight ranging from 40-45 g (right panel). The trend for the ethanol fed mice was different as a decrease in weight was observed (left panel). Here, the final weight ranged from 34-36 g. Pair 1 and 2; controls. Pair 3; 0/ki.

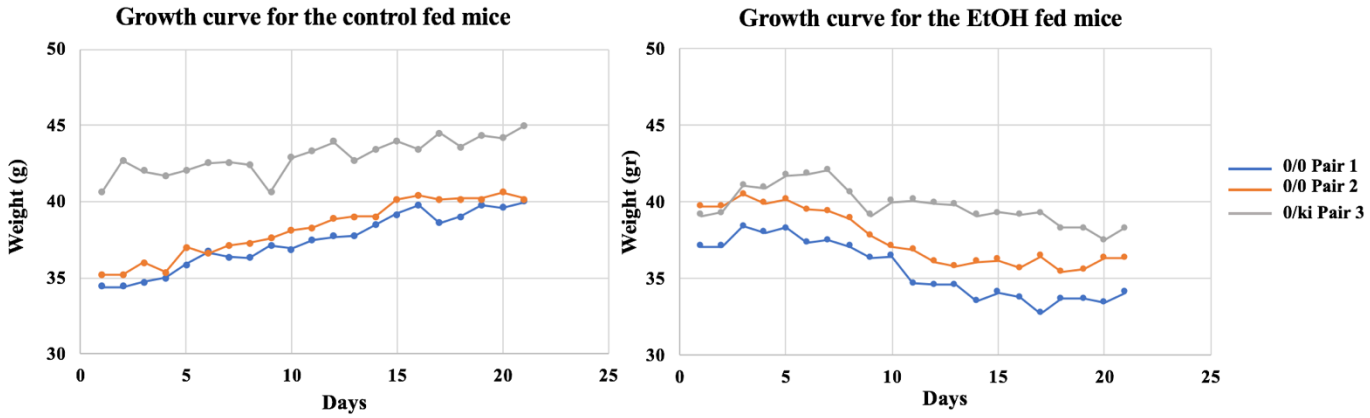

Appendix 3. Testing different epitope retrieval techniques for the CEL-HYB antibody. The heat-induced epitope retrieval (HIER), proteolytic induced epitope retrieval (PIER) and a detergent based epitope retrieval protocol using SDS were tested for the CEL-HYB antibody (5 µg/ml) on control (0/0) and CEL-HYB1 (0/ki) mouse pancreatic tissue. Brown indicated positive staining and the nuclei are stained blue with hematoxylin. To test the HIER method, a tris (pH 9), a citrate (pH 6) and a glycine buffer (pH 3.5) was used, as this covers a wide pH range. Here, the citrate-based buffer showed strong and specific staining compared to the tris and glycine buffer. Proteinase K of two concentrations (2 and 20 µg/ml) was also tested in addition to 1 % SDS. All images were acquired with a Leica DM2000LED microscope with 20x magnification.

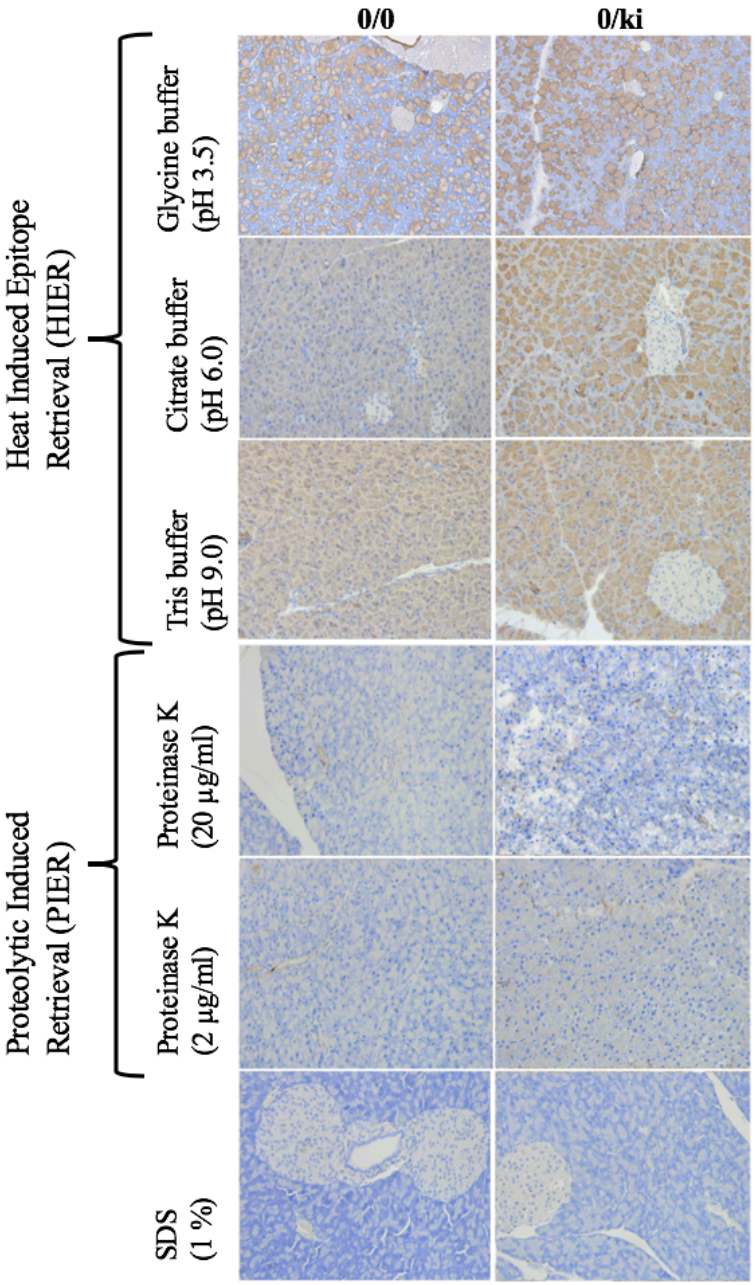

Appendix 4. Effect of different salt concentrations in the antibody diluent. . Epitope retrieval was performed using a citrate buffer (see Appendix 3) and the CEL-HYB antibody was diluted in either low salt (75 mM NaCl) or high salt (150 mM NaCl). Here, a big difference was observed for high and low salt. The staining was enhanced with a high salt containing antibody diluent and the background detected was higher with low salt. Therefore, a high salt-containing diluent was selected for further use. All images are taken with a Leica DM2000LED microscope with 20x magnification.

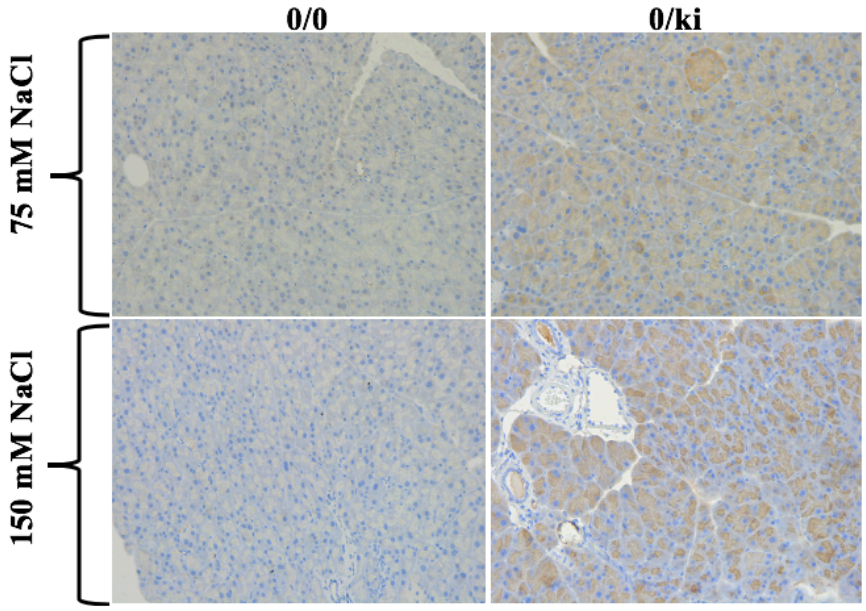

Appendix 5. Testing different citrate-based buffers for optimization of CEL-HYB antibody. Three buffers; citrate (commercial), citrate-EDTA and a sodium-citrate buffer were tested on pancreatic tissue from control (0/0) and CEL-HYB1 (0/ki) mouse. This experiment concluded that the sodium-citrate buffer was most optimal for the antibody as the commercial citrate buffer had a higher degree of background and the citrate-EDTA buffer resulted in staining within the islets. All images are taken by a Leica 2000LED microscope with 20x magnification unless otherwise indicated in the figure.